

## Supporting Information

### Efficient Ethylene/Ethane Separation through Ionic Liquid-confined Covalent Organic Framework Membranes

Xu Liang,<sup>ab</sup> Hong Wu,<sup>abd</sup> Hongliang Huang,<sup>c</sup> Xiaoyao Wang,<sup>ab</sup> Meidi Wang,<sup>ab</sup> Haozhen Dou,<sup>f</sup> Guangwei He,<sup>a</sup> Yanxiong Ren,<sup>ab</sup> Yutao Liu,<sup>ab</sup> Yingzhen Wu,<sup>ab</sup> Shaoyu Wang,<sup>ab</sup> Huilin Ge,<sup>a</sup> Chongli Zhong,<sup>e</sup> Yu Chen,<sup>g</sup> and Zhongyi Jiang<sup>abc\*</sup>

*a.* Key Laboratory for Green Chemical Technology of Ministry of Education, School of Chemical Engineering and Technology, Tianjin University, Tianjin, 300072, China.

*b.* Collaborative Innovation Center of Chemical Science and Engineering (Tianjin), Tianjin, 300072, China.

*c.* Joint School of National University of Singapore and Tianjin University, International Campus of Tianjin University, Binhai New City, Fuzhou, 350207, China.

*d.* Tianjin Key Laboratory of Membrane Science and Desalination Technology, Tianjin University, Tianjin 300072, China.

*e.* State Key Laboratory of Membrane Separation and Membrane Processes, School of Chemistry and Chemical Engineering, Tiangong University, Tianjin, 300387, China.

*f.* Department of Chemical Engineering, University of Waterloo, 200 University Ave. W, Waterloo, Ontario, N2L 3G1, Canada.

*g.* Beijing Synchrotron Radiation Facility, Institute of High Energy Physics, 19B Yuquan Road, Shijingshan District, Beijing, 118852, China.

E-mail: [zhyjiang@tju.edu.cn](mailto:zhyjiang@tju.edu.cn).

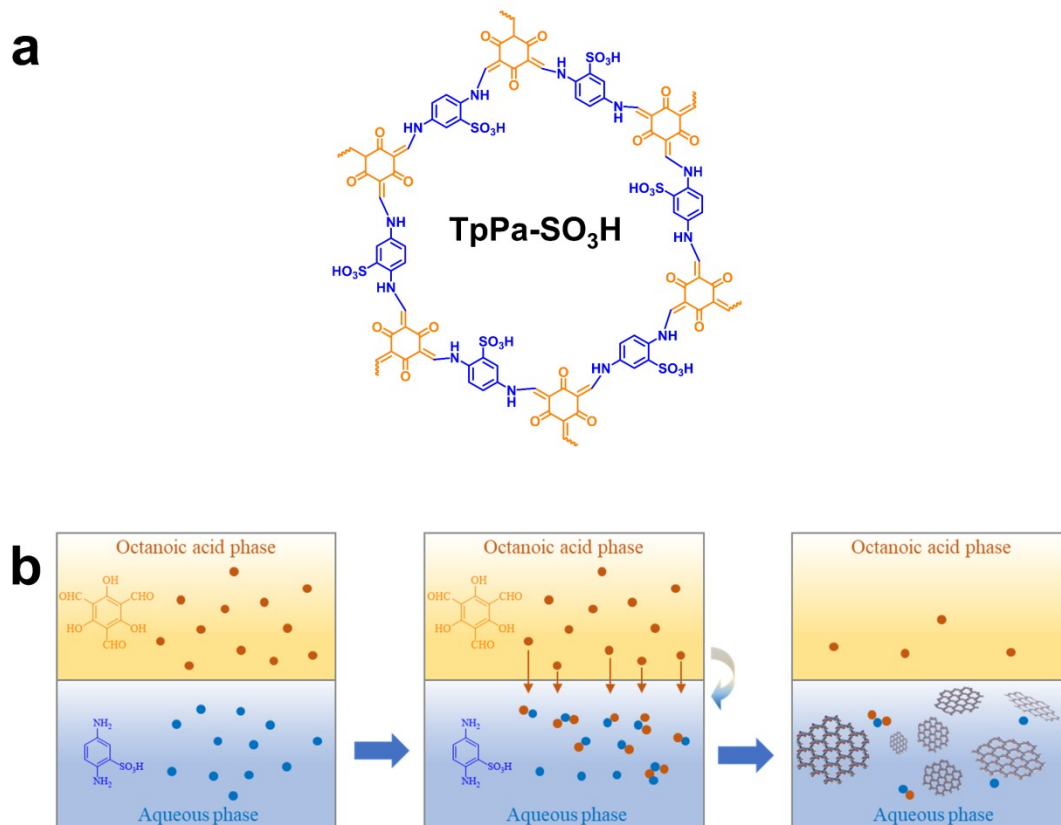


**Figure S1. a**, Chemical structure of TpPa-SO<sub>3</sub>H. Keto-Enol Tautomerism ensures the chemical stability of TpPa-SO<sub>3</sub>H. **b**, Synthesis process of TpPa-SO<sub>3</sub>H nanosheets. The brown and blue dots represent the two monomers, 1,3,5-Triformylphloroglucinol (Tp) and diaminobenzenesulfonic acid (DABA), respectively. Due to the octanoic acid is slightly soluble in water, the Tp monomer will slowly transfers to water phase with the dissolution of octanoic acid. The Tp monomer reacts with DABA monomer in the water phase and the TpPa-SO<sub>3</sub>H nanosheets is formed gradually.



**Figure S2.** The fabrication process of Ag-IL@TpPa-SO<sub>3</sub>H membranes. Firstly, the TpPa-SO<sub>3</sub>H nanosheets are self-assembled into TpPa-SO<sub>3</sub>H membranes by vacuum filtration. Then the Ag-IL/water mixture is spin-coated onto the membrane. Finally, the membranes are vacuum dried to obtain the Ag-IL@TpPa-SO<sub>3</sub>H membranes.

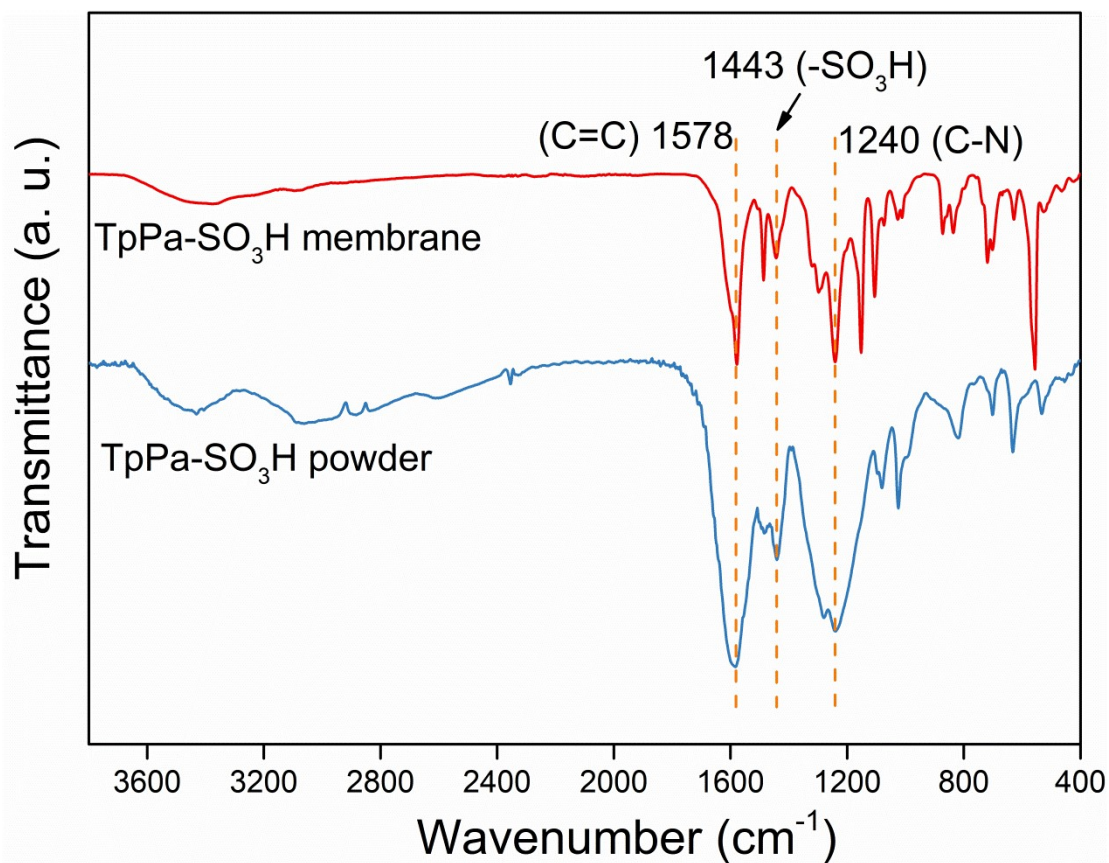


**Figure S3.** FT-IR spectra of TpPa-SO<sub>3</sub>H membrane and TpPa-SO<sub>3</sub>H powder. The FT-IR spectra of TpPa-SO<sub>3</sub>H membrane are measured under Attenuated Total Reflection mode, and the TpPa-SO<sub>3</sub>H powder under Transmittance mode.

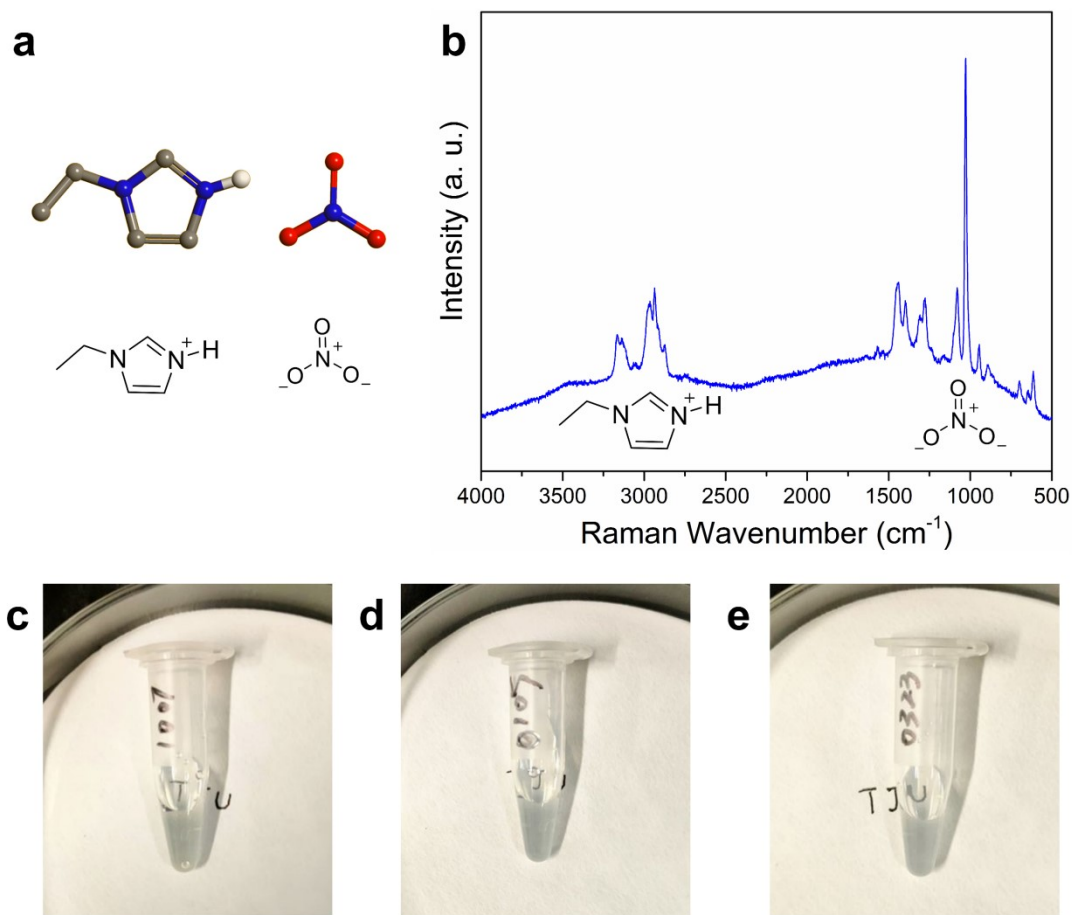


**Figure S4. a,** Chemical structure of the ionic liquid,  $[\text{EIM}]^+[\text{NO}_3]^-$ . **b,** Raman spectra of  $[\text{EIM}]^+[\text{NO}_3]^-$ . The peaks at 2750-3250 and 1000  $\text{cm}^{-1}$  are characteristic peaks of imidazole cations and nitrate ions respectively. **c, d and e,** Photos of the silver ions-containing ionic liquid which was fabricated on October 10<sup>th</sup> 2020, January 5<sup>th</sup> 2021 and March 23<sup>rd</sup> 2021, respectively. The photos were taken on July 1<sup>st</sup>, 2021.

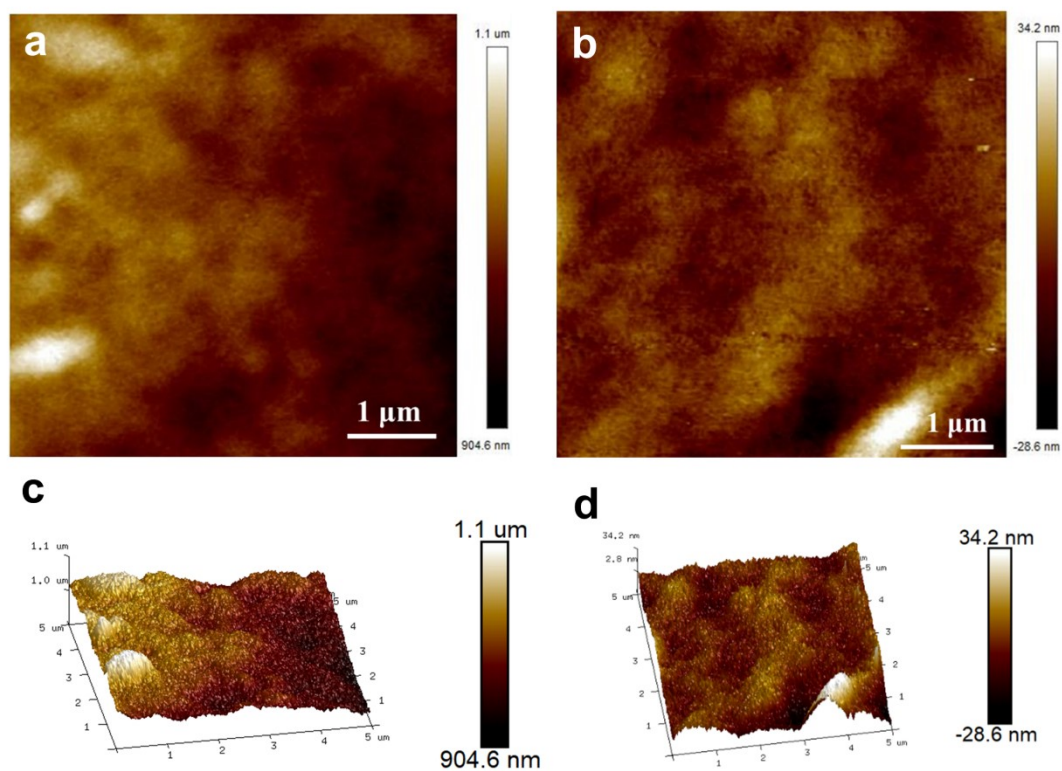


**Figure S5.** AFM images of TpPa-SO<sub>3</sub>H membrane (**a, c**) and Ag-60%IL@TpPa-SO<sub>3</sub>H membrane (**b, d**). The membrane roughness did not change significantly as the increase of Ag-IL proportion.

**Table S1. Roughness of Ag-X%IL@TpPa-SO<sub>3</sub>H membranes with different IL content from AFM characterization.**

Proportion	0%	20%	40%	60%	80%	100%
Rq (nm)	11.97	13.70	11.93	7.14	14.70	9.78
SD(Rq)	1.58	0.50	1.02	1.22	2.38	0.16
Ra (nm)	9.54	10.10	9.54	4.92	11.34	7.82
SD(Ra)	1.10	0.60	0.77	0.39	1.75	0.14

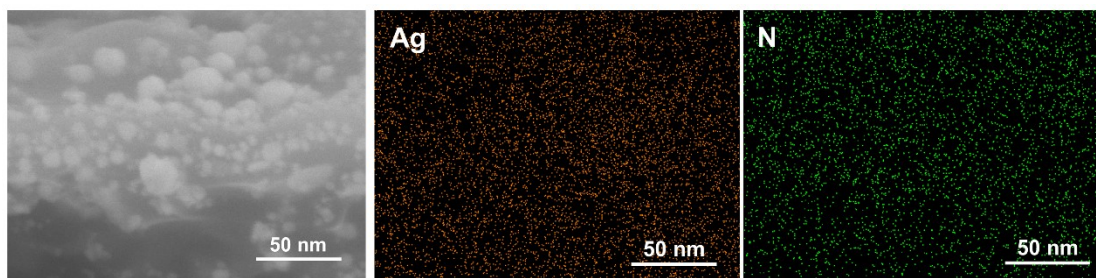


**Figure S6.** Element mapping analysis by energy dispersive X-ray spectroscopy (EDS) of the cross-sectional Ag-60%IL@TpPa-SO<sub>3</sub>H membrane.

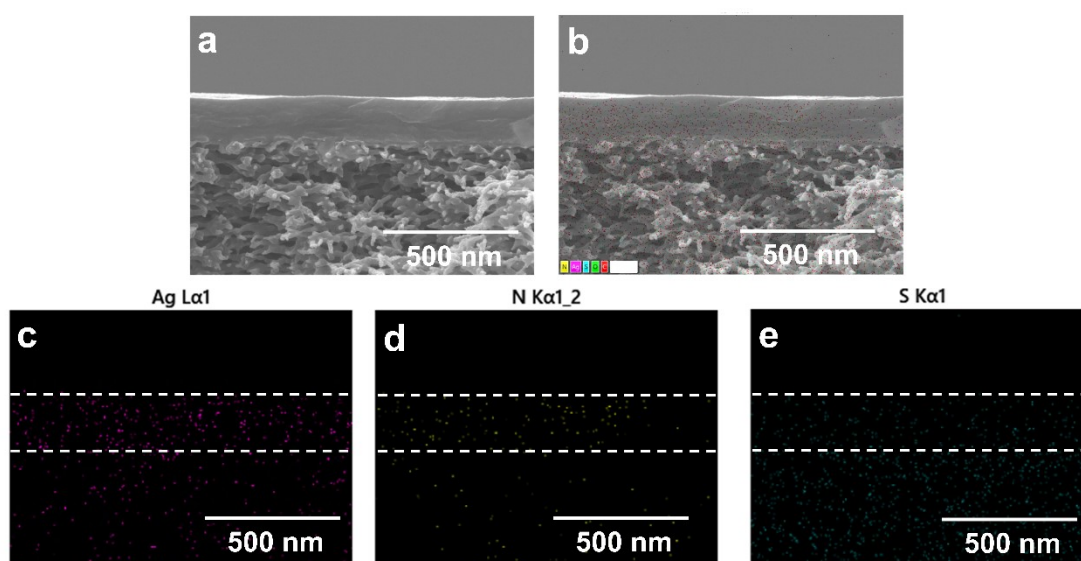


**Figure S7.** Element mapping analysis of the Ag-60%IL@TpPa-SO<sub>3</sub>H membrane and the PES substrate. Fig. **a** and **b** show the scanned area. Fig. **c**, **d** and **e** show the elemental distribution of Ag, N and S, respectively. Ag is the characteristic element of ionic liquid, and N is the characteristic element of COF and ionic liquid. Ag and N elements show weaker signal in the PES substrate, indicating the COF nanosheets and ionic liquid are mainly concentrated in the skin layer of the membrane. The distribution of S element also shows a slight gradient distribution, which is due to the higher S density of PES than that of COF nanosheets.

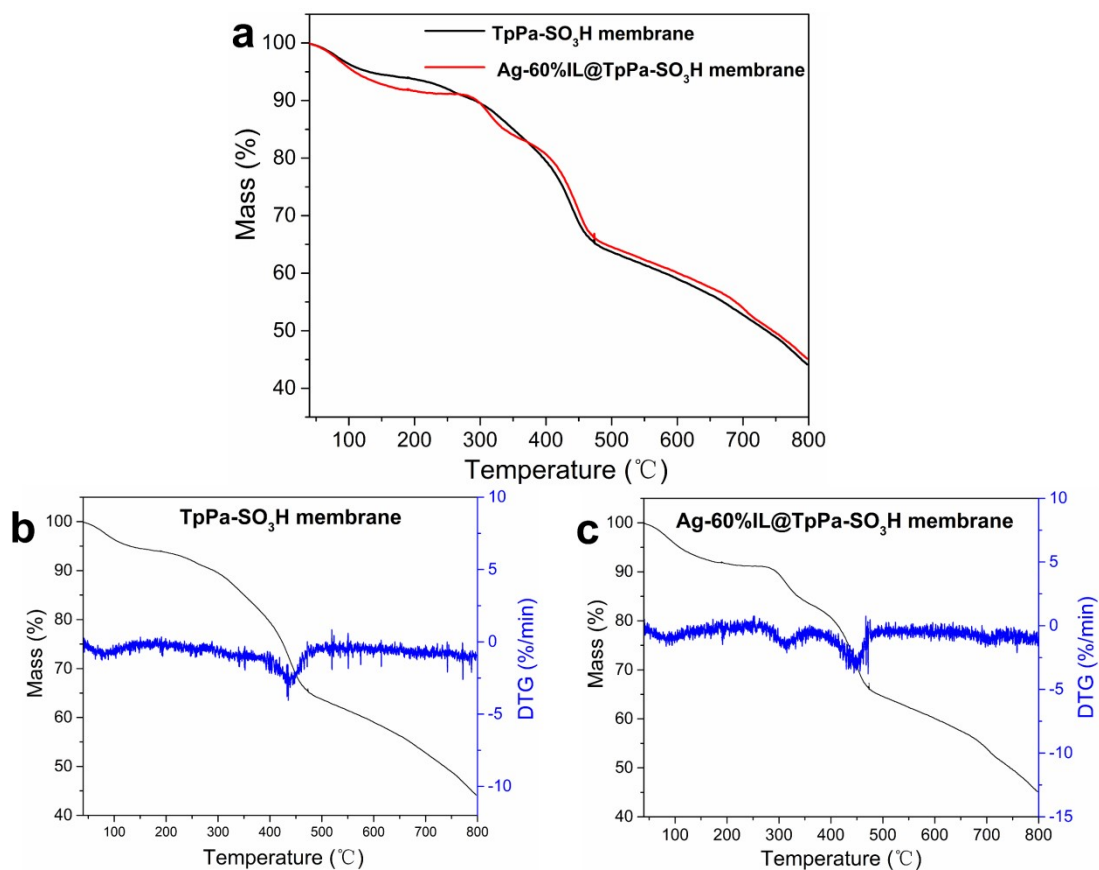


**Figure S8.** TGA analysis of TpPa-SO<sub>3</sub>H membrane and Ag-60%IL@TpPa-SO<sub>3</sub>H membrane from 40 to 800 °C at a heating rate of 10 °C/min<sup>-1</sup> under N<sub>2</sub> atmosphere. The first weight loss (40-100 °C) is related to the loss of absorbed water. The weight loss from 300 to 350 °C of the Ag-60%IL@TpPa-SO<sub>3</sub>H membrane is due to the decomposition of ionic liquid. The weight loss in the range of 400-500 °C is related to the decomposition of COF membranes.

### ***Supporting notes:***

#### ***ICP analysis***

6, 7, 14, 16, and 18 mg of Ag-20, 40, 60, 80, and 100%IL@TpPa-SO<sub>3</sub>H membrane were ground into powder. Then the powder was calcined at 800 °C for 24 h to completely remove carbon element. The collected gray powder was dissolved with 1 ml concentrated nitric acid. Finally, the solution was diluted 200 times for ICP analysis. Experiment was conducted by a VISTA-MPX Inductive Coupled Plasma Emission Spectrometer. The mass fraction of Ag in diluent is 6.752, 5.983, 9.277, 9.227 and 7.146 ppm respectively. Accordingly, the Ag mass fraction in Ag-20, 40, 60, 80, and 100%IL@TpPa-SO<sub>3</sub>H membrane were 22.5 wt%, 17.1 wt%, 13.3 wt%, 11.5 wt%, and 7.9 wt% respectively, showing a decrease with the increase of ionic liquid content.

#### ***Dye rejection***

The membrane was loaded in a filtration cell with effective diameter of 1.4 cm. The dye rejection performance of membrane was evaluated at 4.5 bar with about 80 ppm water solution of Alcian blue (AB) and Methyl blue (MB). Ultraviolet-visible spectrophotometer was applied to analyze the dye concentration. The maximum absorption wavelength of AB and MB are 623 nm and 583 nm based on the UV spectra. By evaluating the UV absorbance of 0, 1, 10, 30, 60, 100 ppm water solution of AB and MB at 623 nm and 583 nm respectively, it was found that there is accurate linear correlation between solute concentration (C) and absorbance (A) from 0 to 100 ppm (Figure S9 c, d, Table S2). Thus, the dye rejection rate can be calculated by following equation:

$$R = \left( 1 - \frac{C_{feed}}{C_{filtrate}} \right) \times 100\% = \left( 1 - \frac{A_{feed}}{A_{filtrate}} \right) \times 100\%$$

The UV absorbance of feed and filtrate at 623 nm in AB rejection is 2.624 and 0.007 respectively. For the feed and filtrate in MB rejection, the UV absorbance at 583 nm is 1.919 and 0.023 respectively (Figure S9 a, b). Accordingly, the AB and MB rejection rates of the TpPa-SO<sub>3</sub>H membrane are 99.7 % and 98.8 %, respectively.

#### ***Gas sorption tests***

*Preparation of the powdered samples:* Firstly, COF layer with a diameter of 2 cm was fabricated with 2.1 ml TpPa-SO<sub>3</sub>H nanosheet dispersion. Then, 0.21 ml Ag-IL solution was spin-coated into the membrane (15 µl for each time, totally 14 times). Due to the increased thickness, the skin layer can be easily exfoliated from the PES substrates. Considering the loss of the nanosheets in the vacuum assisted assembly process, over 50 mg sample can be obtained by fabricating 30 to 40 pieces of the skin layers. The layers were then ground into powder for gas sorption tests.

*NLDFT calculation:* The NLDFT calculation was conducted using software BELMaster7 matched with BELSORP-Max apparatus. N<sub>2</sub>/77K was set as Adsorptive/Temp. Cylinder was chosen as the Model. Graphitic carbon ads. branch was chosen as the Adsorbent. Adsorption was chosen as the Data. Log-normal was chosen as Fitting method and the Number of Peaks was set as 2 to 5 which is determined according to the fitting degree of the fitting curves. For Ag-0%, 20%, 40%, 60%, 80%IL@TpPa-SO<sub>3</sub>H samples, the Number of Peaks are 5, 2, 3, 3, 3, respectively.

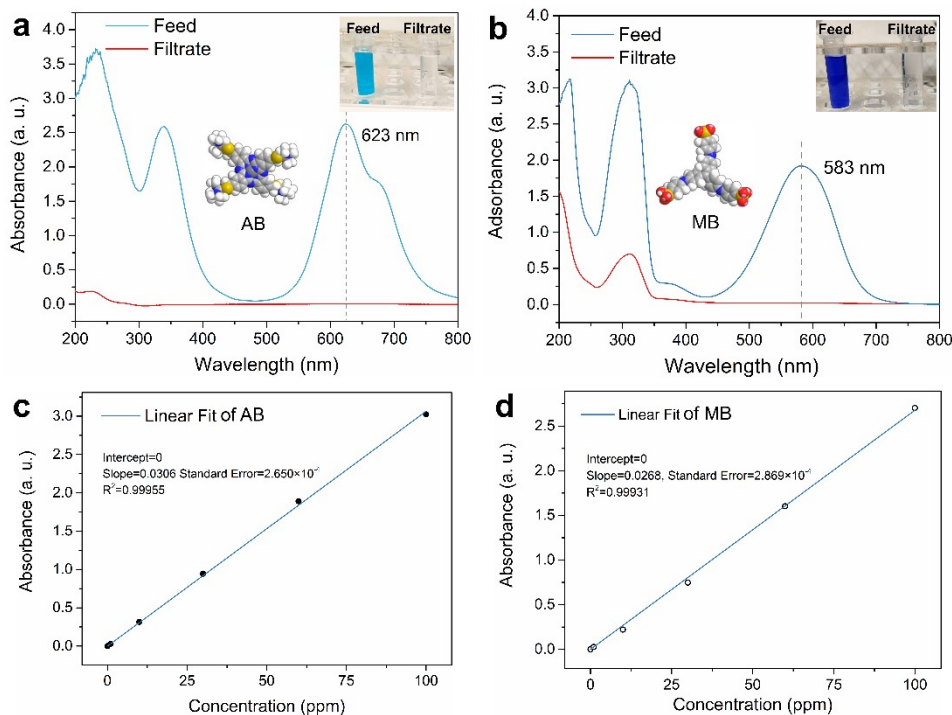


**Figure S9.** Ultraviolet-visible absorption spectra of (a) Alcian blue (AB) and (b) Methyl blue (MB) in feed and filtrate of TpPa-SO<sub>3</sub>H membrane. Inset: Digital photographs of feed and filtrate (top right) and molecular structure of AB and MB. c, Linear fit of AB concentration (ppm) and the UV absorbance (a. u.) at 623 nm. d, Linear fit of MB concentration (ppm) and the UV absorbance (a. u.) at 583 nm.

**Table S2.** Summary of AB and MB concentration and the corresponding UV absorbance.

$C_{AB}$ /ppm	0	1	10	30	60	100
$A_{623\text{ nm}}$ /a. u.	0	0.03	0.316	0.945	1.891	3.024
$C_{MB}$ /ppm	0	1	10	30	60	100
$A_{583\text{ nm}}$ /a. u.	0	0.026	0.221	0.747	1.603	2.703

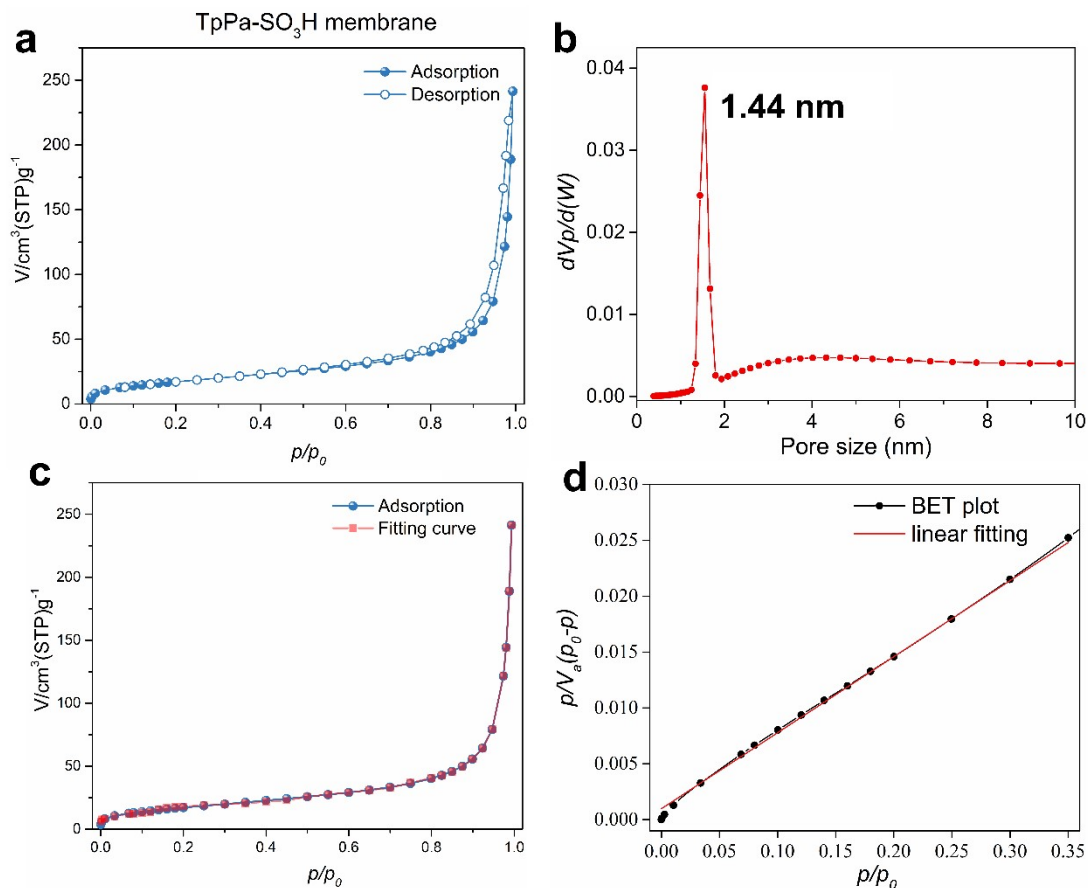


**Figure S10.**  $N_2$  adsorption analysis of TpPa-SO<sub>3</sub>H membrane at 77 K. **a**,  $N_2$  adsorption and desorption isotherms. **b**, Channel size distribution of TpPa-SO<sub>3</sub>H membrane based on nonlocal density function theory (NLDFT). **c**, Fitting curve from NLDFT calculation of the channel size distribution. **d**, BET plot of the adsorption isotherm. In the linear fitting, the start point is the 5th and the end point is the 13th. The linear slope is  $6.647 \times 10^{-2}$  and the intercept is  $1.3326 \times 10^{-3}$  with correlation coefficient of 1.0000 and C of 50.879. As a result, the  $S_{\text{BET}}$  is 64.2  $\text{m}^2/\text{g}$ .

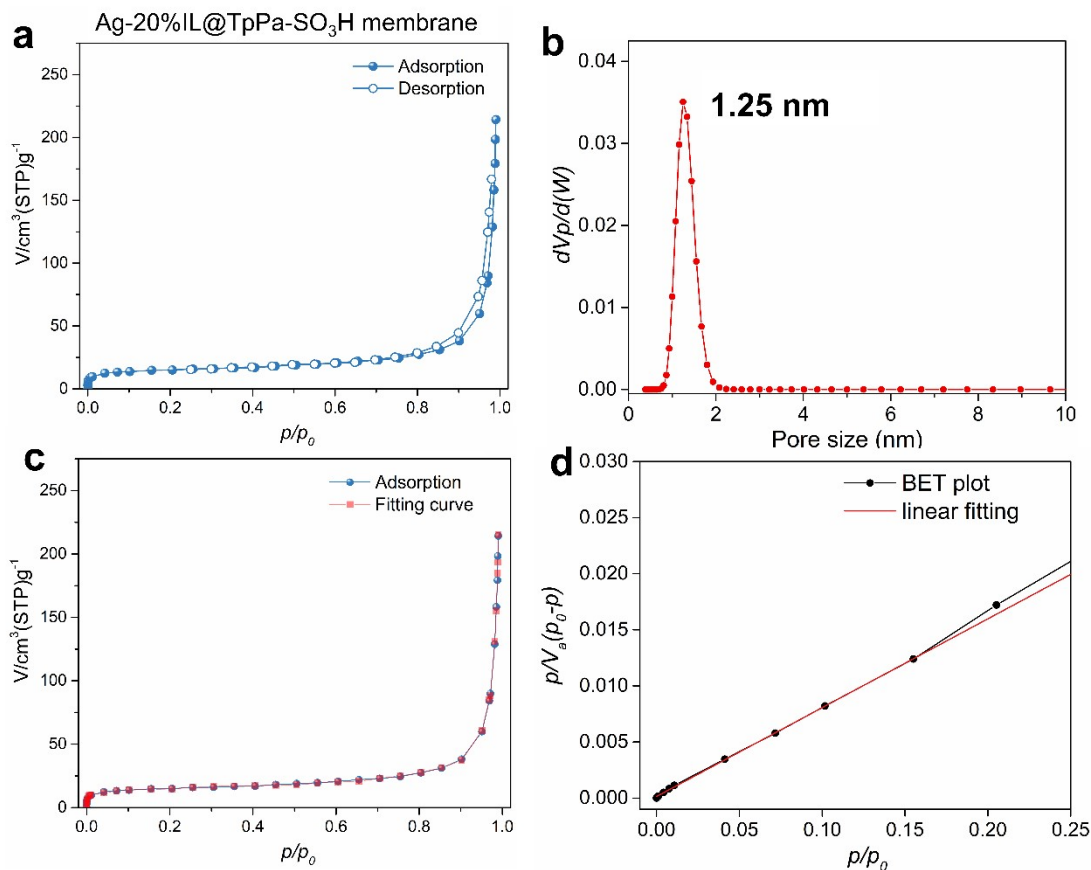


**Figure S11.**  $N_2$  adsorption analysis of Ag-20%IL@TpPa-SO<sub>3</sub>H membrane at 77 K. **a**,  $N_2$  adsorption and desorption isotherms. **b**, Channel size distribution of TpPa-SO<sub>3</sub>H membrane based on NLDFT. **c**, Fitting curve from NLDFT calculation of the channel size distribution. **d**, BET plot of the adsorption isotherm. In the linear fitting, the start point is the 3th and the end point is the 12th. The linear slope is  $7.92 \times 10^{-2}$  and the intercept is  $1.40 \times 10^{-4}$  with correlation coefficient of 0.9998 and C of 567.51. As a result, the  $S_{BET}$  is  $54.9 \text{ m}^2/\text{g}$ .

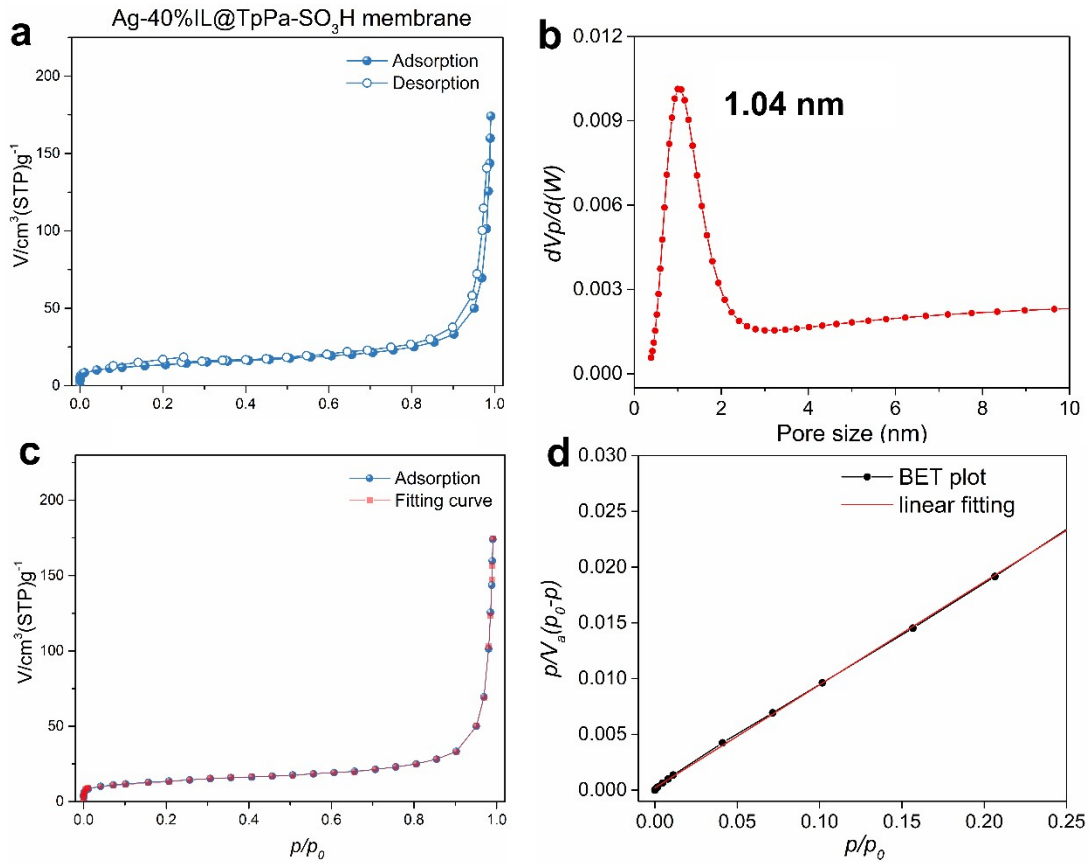


**Figure S12.**  $N_2$  adsorption analysis of Ag-40%IL@TpPa-SO<sub>3</sub>H membrane at 77 K. **a**,  $N_2$  adsorption and desorption isotherms. **b**, Channel size distribution of TpPa-SO<sub>3</sub>H membrane based on nonlocal NLDFT. **c**, Fitting curve from NLDFT calculation of the channel size distribution. **d**, BET plot of the adsorption isotherm. In the linear fitting, the start point is the 3th and the end point is the 12th. The linear slope is  $9.23 \times 10^{-2}$  and the intercept is  $2.08 \times 10^{-4}$  with correlation coefficient of 0.9996 and C of 445.83. As a result, the  $S_{\text{BET}}$  is 47.0  $\text{m}^2/\text{g}$ .

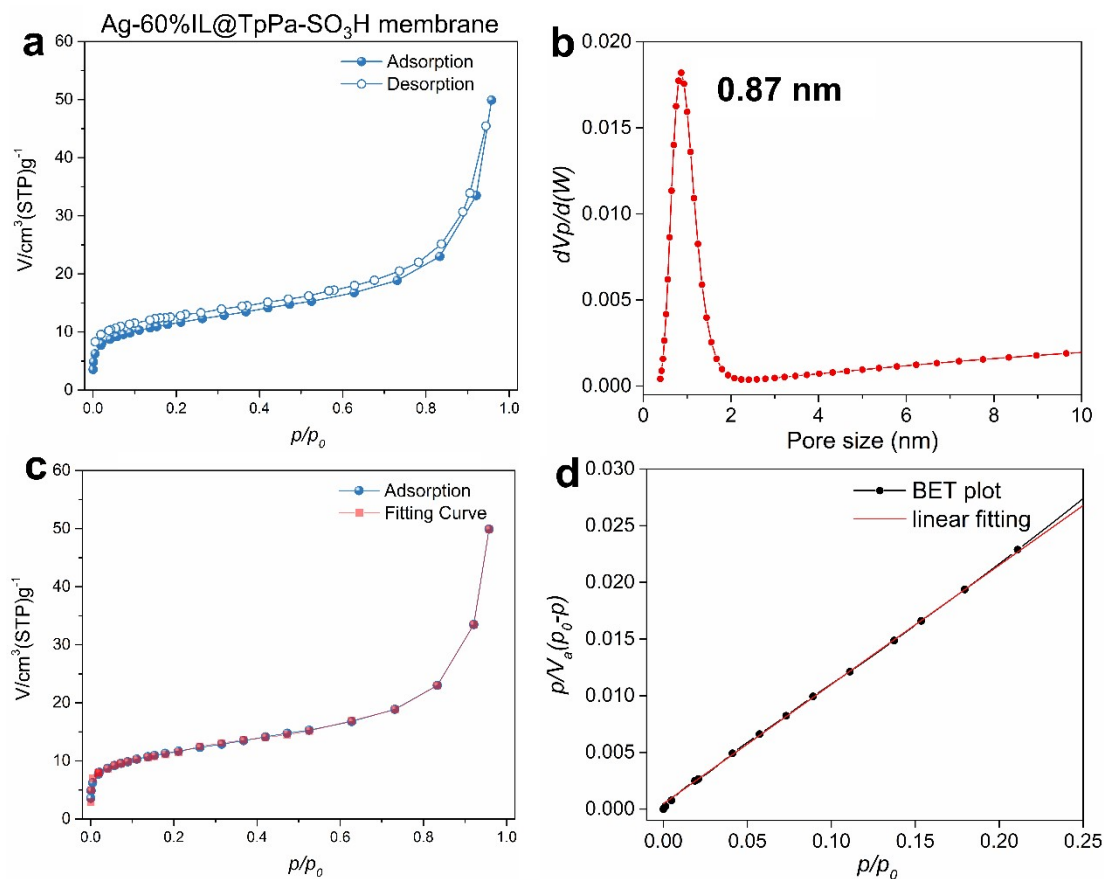


**Figure S13.**  $N_2$  adsorption analysis of Ag-60%IL@TpPa-SO<sub>3</sub>H membrane at 77 K. **a**,  $N_2$  adsorption and desorption isotherms. **b**, Channel size distribution of TpPa-SO<sub>3</sub>H membrane based on NLDFT. **c**, Fitting curve from NLDFT calculation of the channel size distribution. **d**, BET plot of the adsorption isotherm. In the linear fitting, the start point is the 3th and the end point is the 13th. The linear slope is 0.105 and the intercept is  $4.77 \times 10^{-4}$  with correlation coefficient of 0.9999 and C of 221.48. As a result, the  $S_{BET}$  is 41.2 m<sup>2</sup>/g.

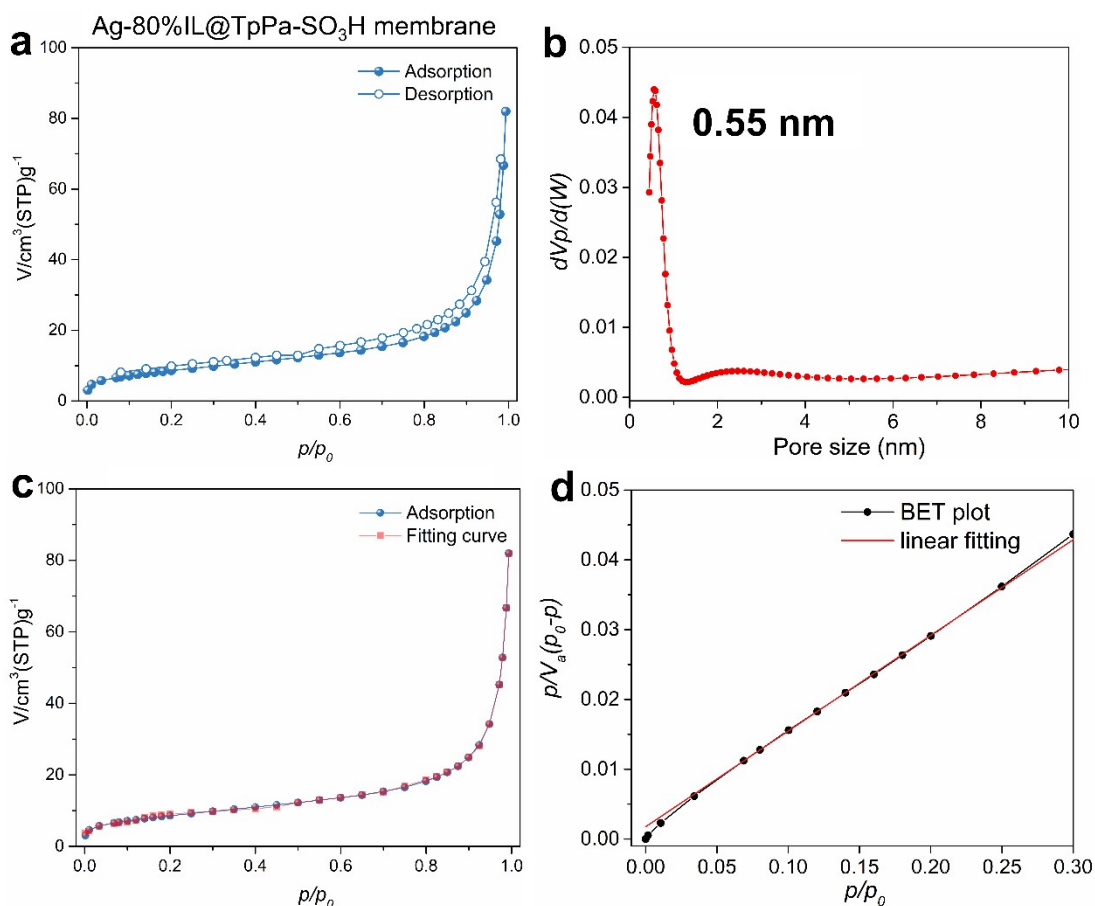


**Figure S14.**  $N_2$  adsorption analysis of Ag-80%IL@TpPa-SO<sub>3</sub>H membrane at 77 K. **a**,  $N_2$  adsorption and desorption isotherms. **b**, Channel size distribution of TpPa-SO<sub>3</sub>H membrane based on NLDFT. **c**, Fitting curve from NLDFT calculation of the channel size distribution. **d**, BET plot of the adsorption isotherm. In the linear fitting, the start point is the 4th and the end point is the 12th. The linear slope is 0.137 and the intercept is  $1.76 \times 10^{-3}$  with correlation coefficient of 0.9999 and C of 79.077. As a result, the  $S_{\text{BET}}$  is 31.341  $\text{m}^2/\text{g}$ .

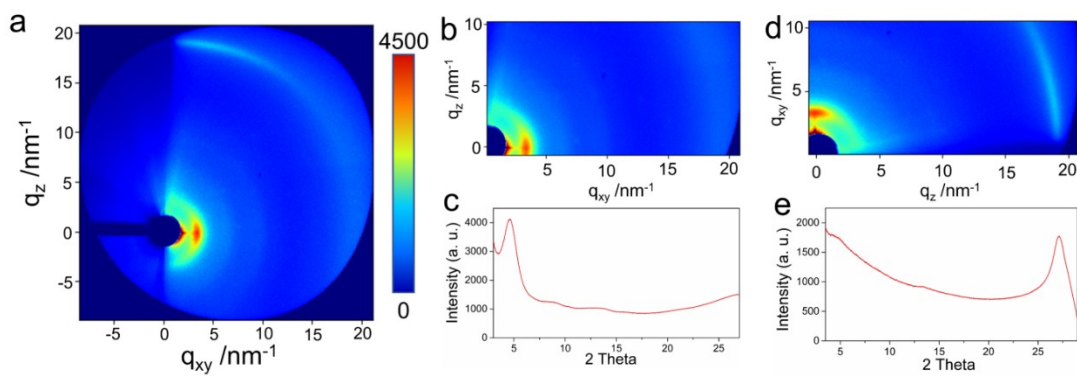


**Figure S15.** **a**, GIWAXS data of TpPa-SO<sub>3</sub>H membrane. **b, c**, Projection of GIWAXS data sets near  $q_z=0$ , which gave only the peak at 2 Theta of about 4.7°, corresponding to the (100) reflection plane. **d, e**, Projection of GIWAXS data sets near  $q_{xy}=0$ , which gave only the peak at 2 Theta of about 27°, corresponding to the (001) reflection plane.

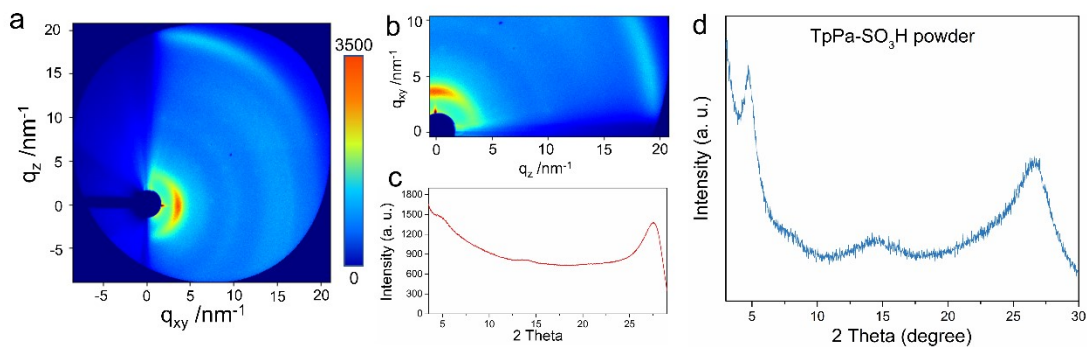


**Figure S16.** **a**, GIWAXS data of Ag-60%IL@TpPa-SO<sub>3</sub>H membrane. **b**, **c**, projection of GIWAXS data sets near  $q_{xy}=0$ . **d**, XRD spectra of TpPa-SO<sub>3</sub>H powder. The diffraction peaks at  $2\theta = 4.7^\circ$  and  $27^\circ$  are assigned to the (100) and (001) planes, respectively. The (100) lattice plane reflects the growth of TpPa-SO<sub>3</sub>H layer along two-dimensional plane. The (001) lattice plane reflects the  $\pi$ - $\pi$  stacking of TpPa-SO<sub>3</sub>H layer.

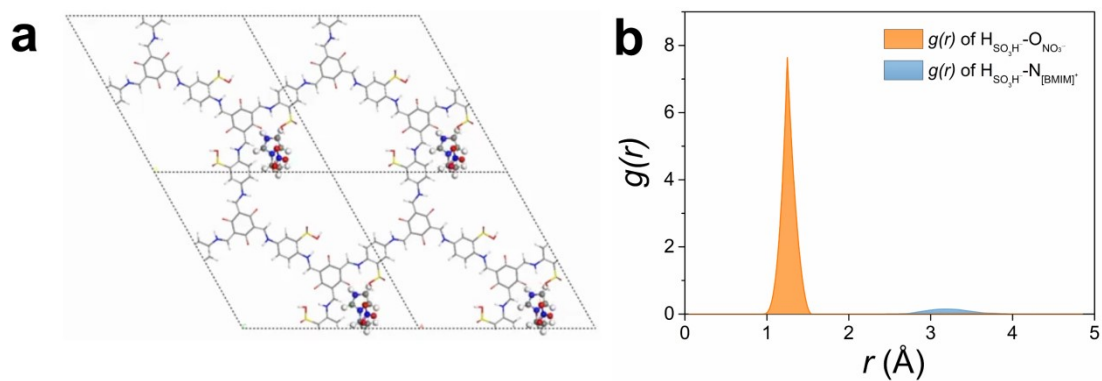


**Figure S17. a**, AIMD simulation snapshot of IL in the channel of TpPa-SO<sub>3</sub>H. The ionic liquid was adsorbed near sulfonate throughout the simulation process. **b**, Radical distribution functions (RDFs) of [EIM]<sup>+</sup>[NO<sub>3</sub>]<sup>-</sup> in the TpPa-SO<sub>3</sub>H framework. The white, grey, blue, red, and yellow spheres in the atomic graphs refer to the H, C, N, O, and S, respectively.

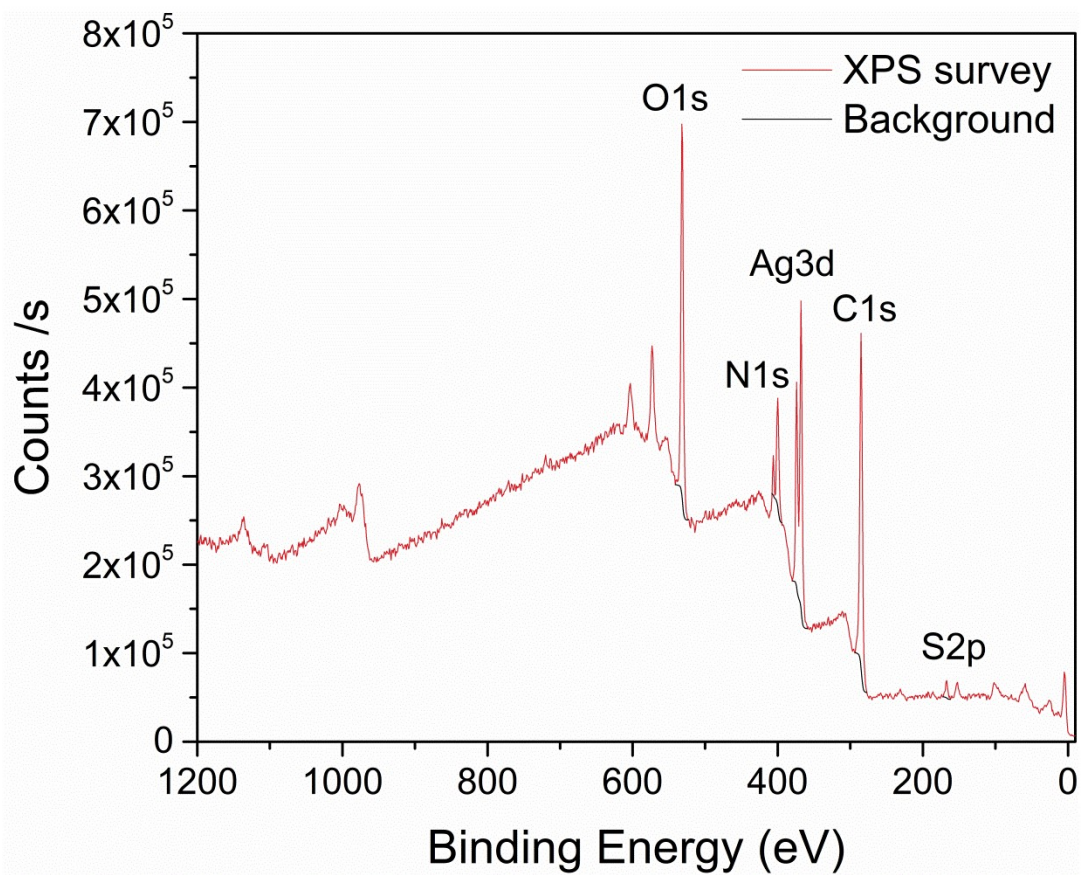


**Figure S18.** The full scan XPS spectra of Ag-60%IL@TpPa-SO<sub>3</sub>H membrane. The Ag3d peaks at about 350 eV indicated the successful introduction of silver ions into the membrane. Charged compensation has been conducted for XPS data.

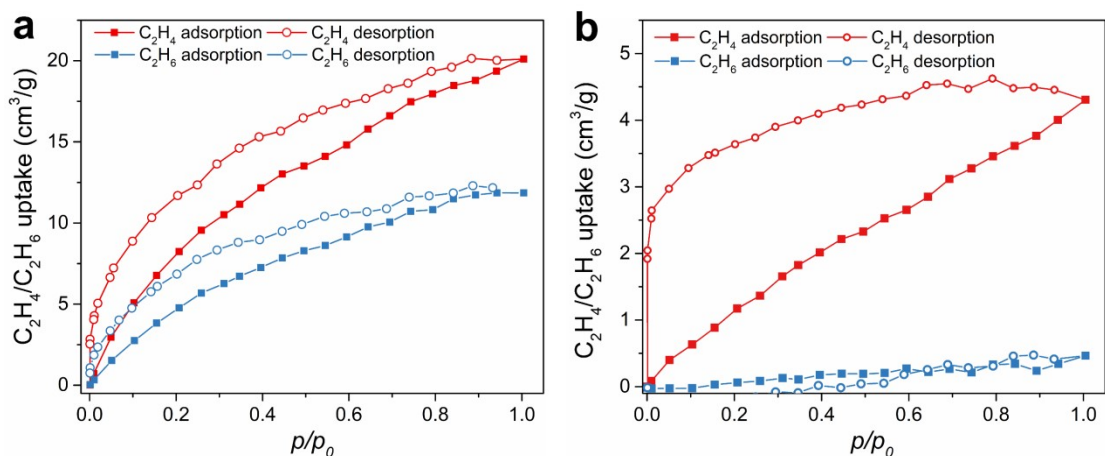


**Figure S19. The  $C_2H_4$  and  $C_2H_6$  adsorption and desorption isotherms of a,  $TpPa-SO_3H$  membrane and b,  $Ag-60\%IL@TpPa-SO_3H$  membrane at 298 K.** For  $TpPa-SO_3H$  membrane, the adsorption capacities of ethylene and ethane at atmospheric pressure are 20.02  $cm^3/g$  and 11.83  $cm^3/g$ . The sample shows no obvious adsorption selectivity for ethylene and ethane. For  $Ag-60\%IL@TpPa-SO_3H$  membrane, the adsorption capacities of ethylene and ethane at atmospheric pressure are 4.30  $cm^3/g$  and 0.46  $cm^3/g$ , respectively. Besides, the desorption of ethylene showed a large lag. Ethylene is adsorbed and desorbed by chemical reaction while ethane by physical reaction, which means the adsorption and desorption of two molecules belong to different models. Hence the adsorption selectivity can not be calculated. However, the adsorption difference can still be compared by the atmospheric pressure adsorption capacity of the two.

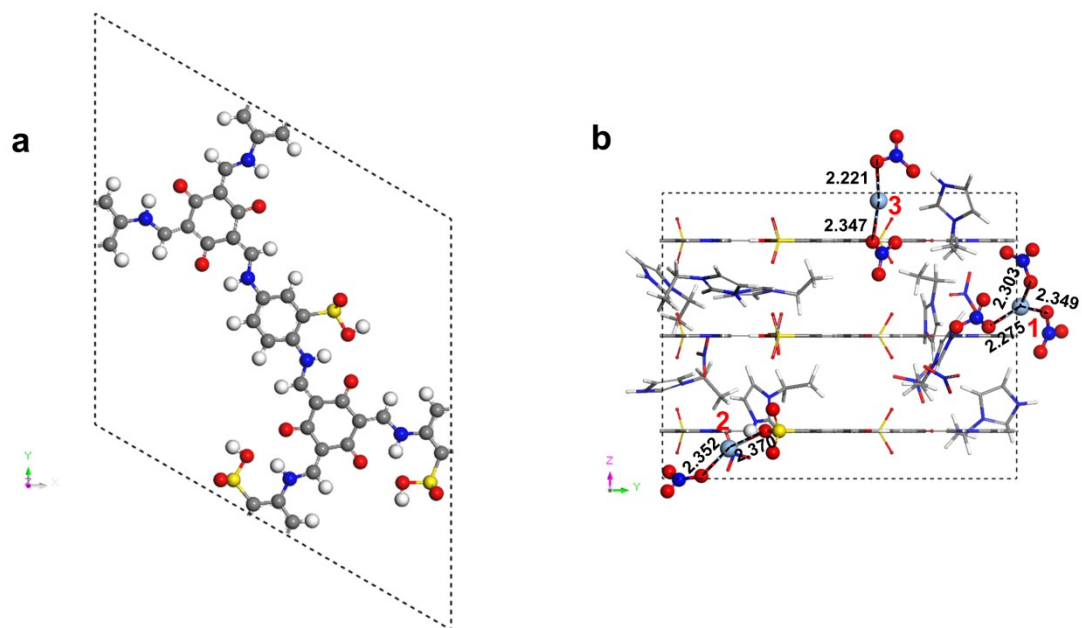


**Figure S20.** AIMD simulation of Ag-IL@TpPa-SO<sub>3</sub>H membrane channels. **a**, Illustration of the crystal structure of TpPa-SO<sub>3</sub>H (top view). **b**, Snapshot of the AIMD-simulated AgNO<sub>3</sub>-[EIM]<sup>+</sup> [NO<sub>3</sub>]<sup>-</sup> @TpPa-SO<sub>3</sub>H structure (the 13510 frame) (side view). The gray, red, yellow, blue, white, and light blue balls or sticks represent the C, O, S, N, H, and Ag atoms, respectively.

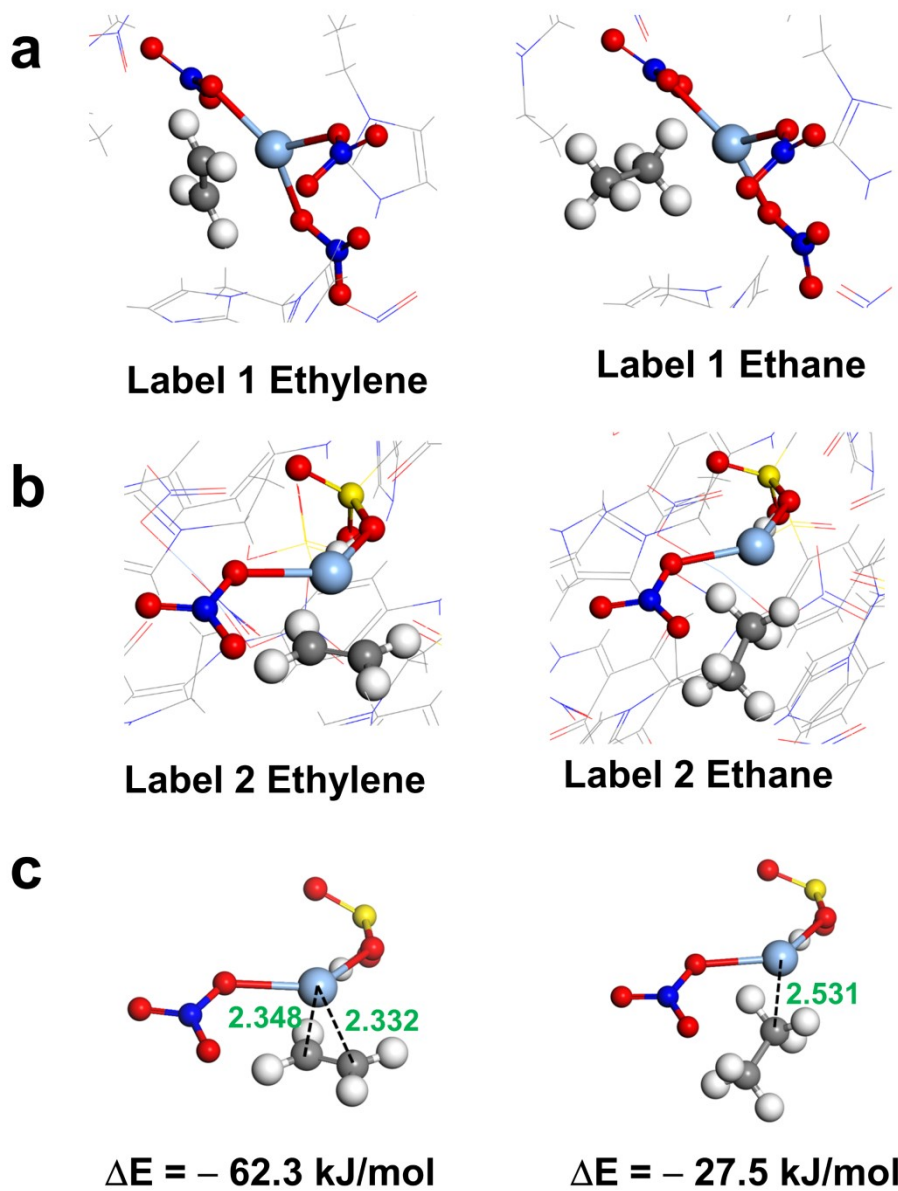


**Figure S21.** **a, b,** the simulation environment of geometry and binding energy optimizations of ethylene or ethane to the silver ions. **c,** optimized structures for ethylene and ethane bound to the silver ions of label 2.

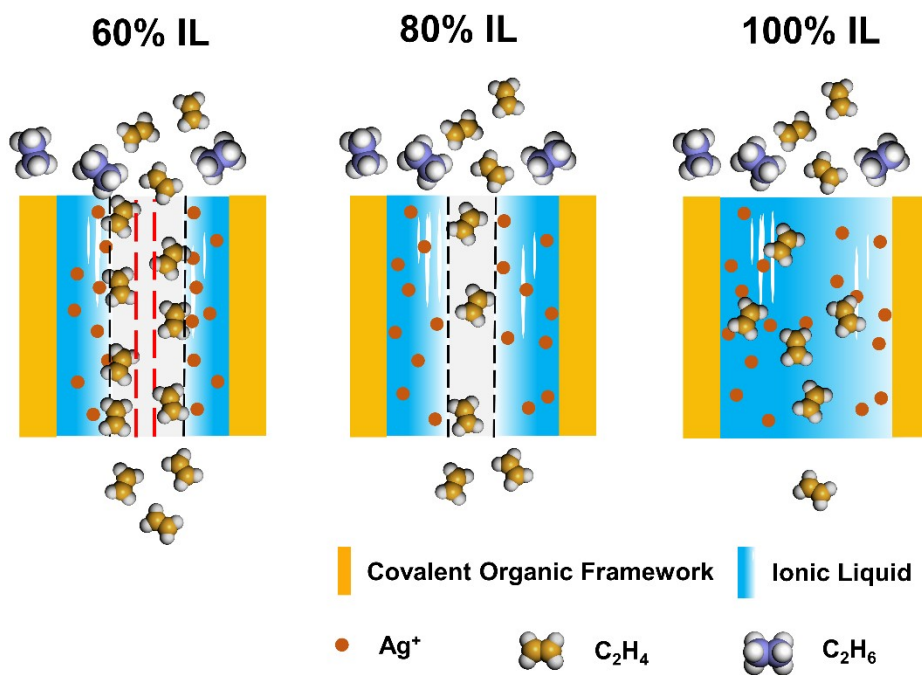


**Figure S22.** Schematic of Ag-60, 80 and 100%IL@TpPa-SO<sub>3</sub>H membrane channels. With the IL content increasing from 60% to 100%, the channel size decreases and finally the IL completely occupies the membrane channels.

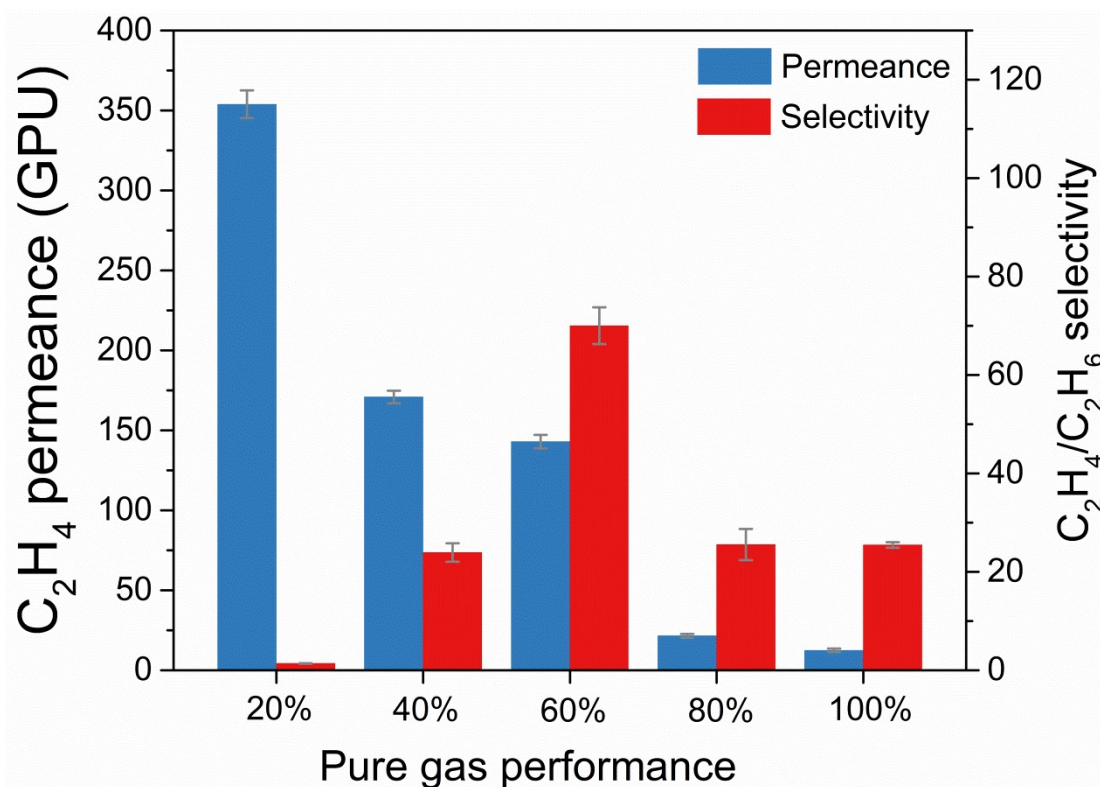


**Figure S23. Performance of Ag-X%IL@TpPa-SO<sub>3</sub>H membranes for pure ethylene and ethane.** The trends of permeance and selectivity are consistent with that of the mixed gas texts. For the same membrane, the permeance is higher while the selectivity is lower than that of the mixed gas text. Experiments were conducted using a temperature of 20±0.5 °C, a constant pressure of 1bar, a feed gas flow rate of 15 ml/min and a sweep gas flow rate of 8 ml/min. Error bars represent standard deviations from duplicate measurements of at least three individual samples.

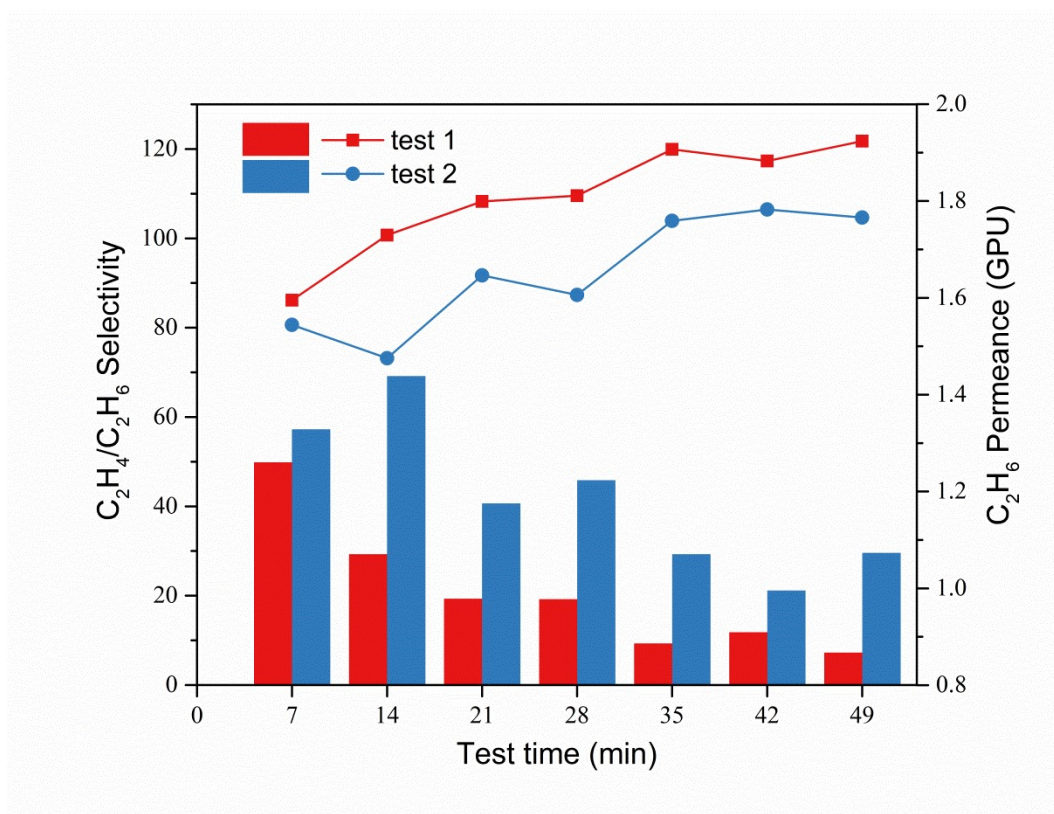


**Figure S24. The performance changes of the Ag-60%IL@TpPa-SO<sub>3</sub>H membranes at initial stage of test.** Tests began immediately after the membranes were placed in the membrane cells and were performed every 7 minutes. The two results of these tests are shown in the figure, both of which show that the ethane permeance decreased and the ethylene/ethane selectivity increased. Experiments were conducted using a temperature of 20±0.5 °C, a constant pressure of 1 bar, a feed gas flow rate of 15 ml/min and a sweep gas flow rate of 8 ml/min.

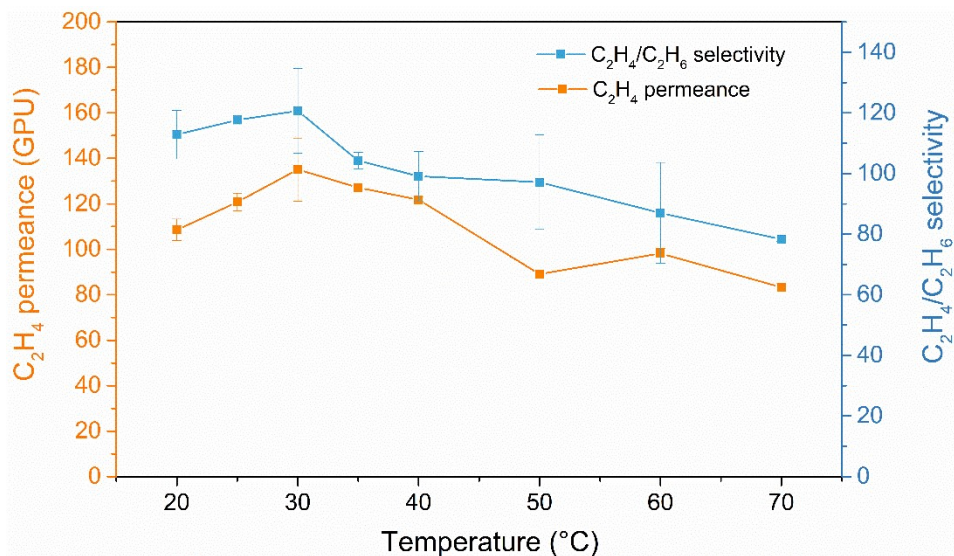


**Figure S25.** The performance changes by temperature of the **Ag-60%IL@TpPa-SO<sub>3</sub>H** membranes. The temperature varies from 20 to 70 °C. Experiments were conducted using a constant pressure of 1bar, a feed gas flow rate of 15 ml/min and a sweep gas flow rate of 8 ml/min. Error bars represent standard deviations from duplicate measurements of at least three individual samples.

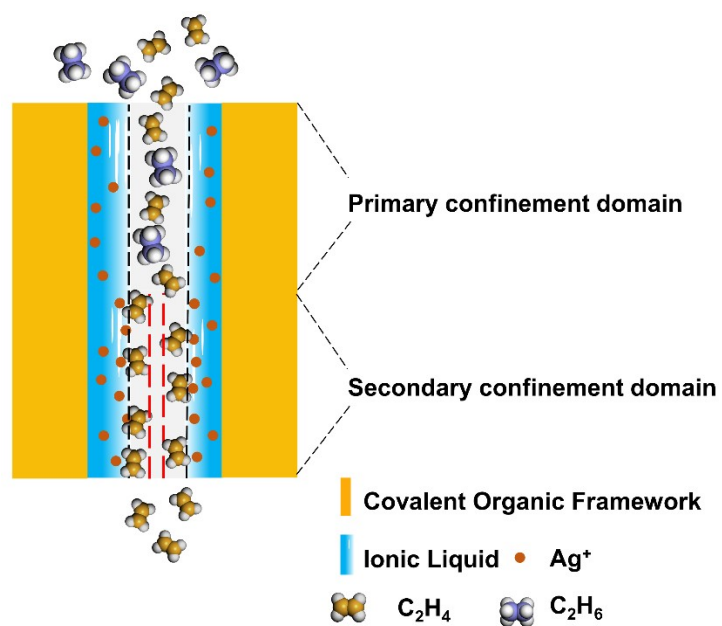


**Figure S26.** Schematic of different domains where the primary confinement effect and the secondary confinement effect happen.

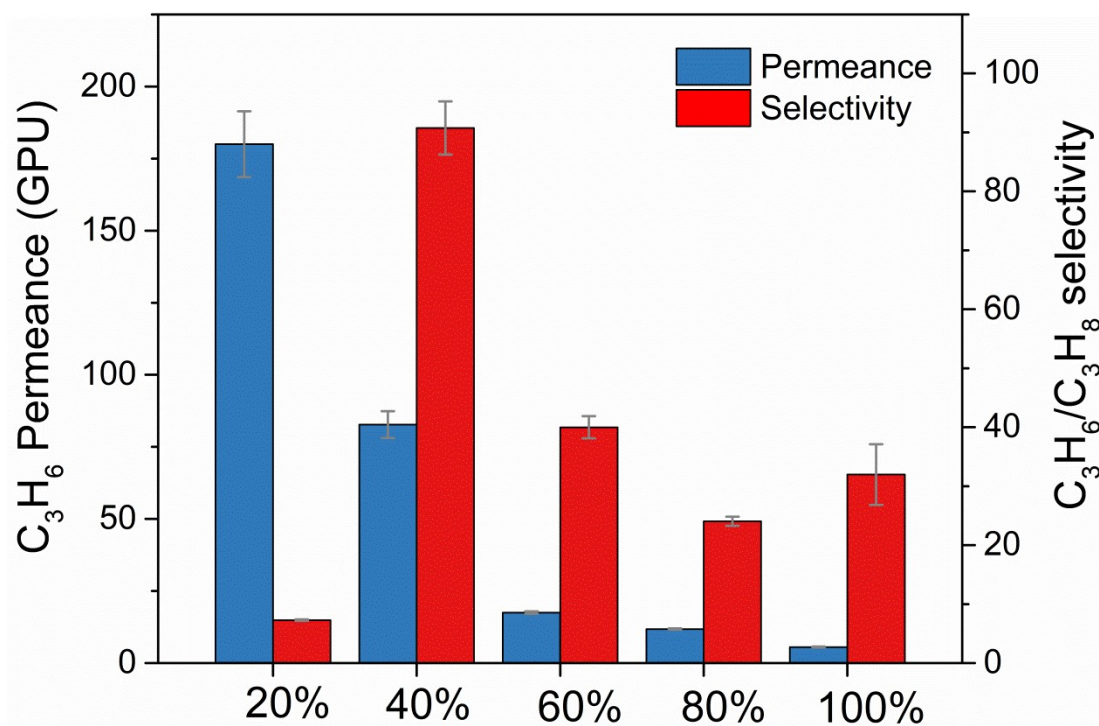


**Figure S27. The performance of the Ag-X%IL@TpPa-SO<sub>3</sub>H membranes for propylene/propane separation.** The performance variation was similar to ethylene/ethane separation, while the highest performance appeared at Ag-40%IL@TpPa-SO<sub>3</sub>H membrane, when the propylene permeance is 82 GPU and the propylene/propane selectivity is 90. Experiments were conducted using a temperature of 20±0.5 °C, a constant pressure of 1 bar, a feed gas flow rate of 15 ml/min and a sweep gas flow rate of 8 ml/min. Error bars represent standard deviations from duplicate measurements of at least three individual samples.

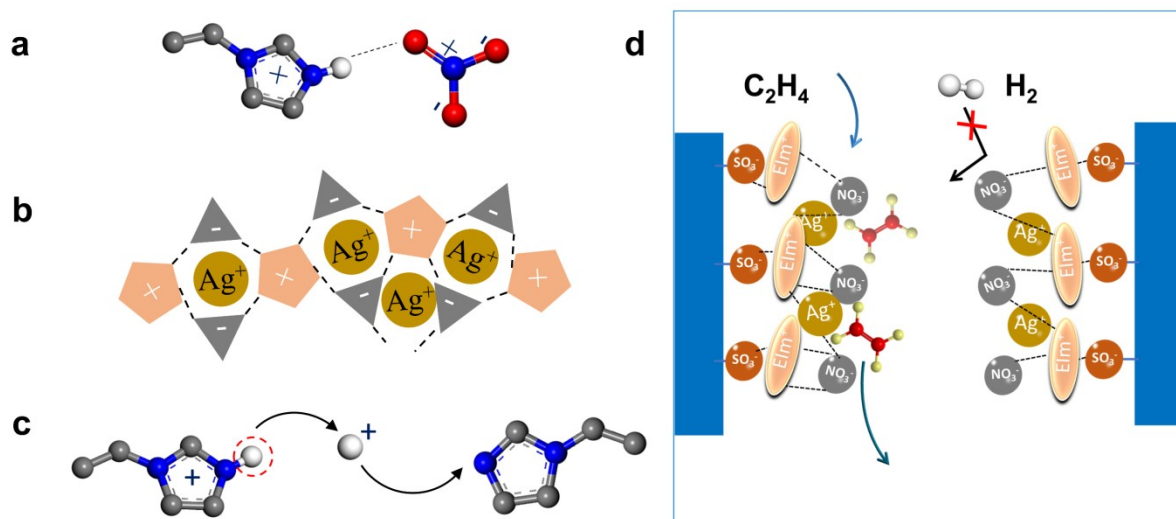


**Figure S28. Mechanism of long-term stability of the membrane under hydrogen atmosphere.** **a, b**, the EIM<sup>+</sup> and NO<sub>3</sub><sup>-</sup> ions are arranged orderly in the membrane channels from the simulation. Ordered hydrogen-bond network will be formed between EIM<sup>+</sup> and NO<sub>3</sub><sup>-</sup> of the ionic liquid, resulting in a high viscosity to prevent silver ions from the reduction of hydrogen. **c**, EIM<sup>+</sup> will dissociate hydrogen protons and provide acidic environment. **d**, schematic of the confinement layer absorbing ethylene molecules and repelling hydrogen molecules.

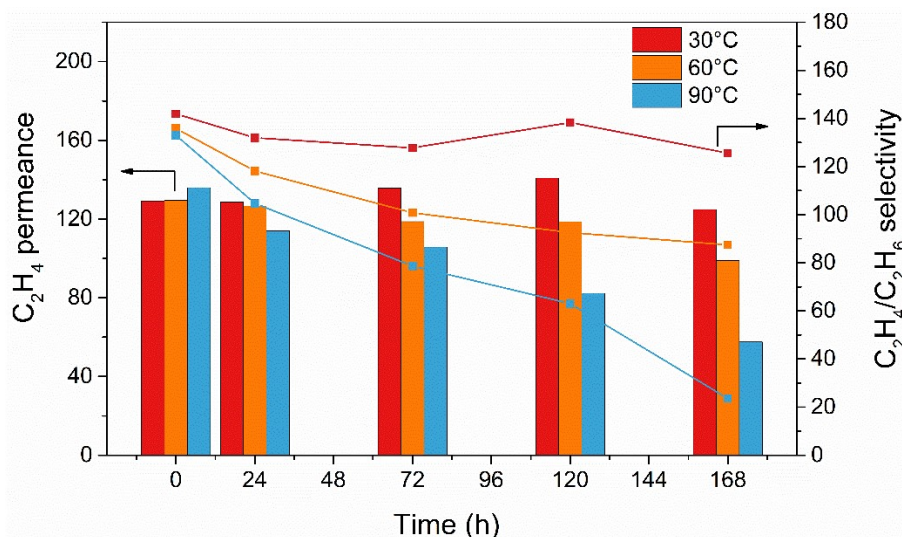


**Figure S29.** Separation performance of Ag-60%IL@TpPa-SO<sub>3</sub>H membranes exposed to hydrogen at 30, 60 and 90 °C, respectively. In order to avoid the change of silver ion activity caused by temperature during the test, we stored the membranes under hydrogen atmosphere and at a specific temperature (30, 60 and 90 °C) for a period of time (0, 24, 72, 120 and 168 hours), and then evaluated the membrane separation performance at 30 °C.

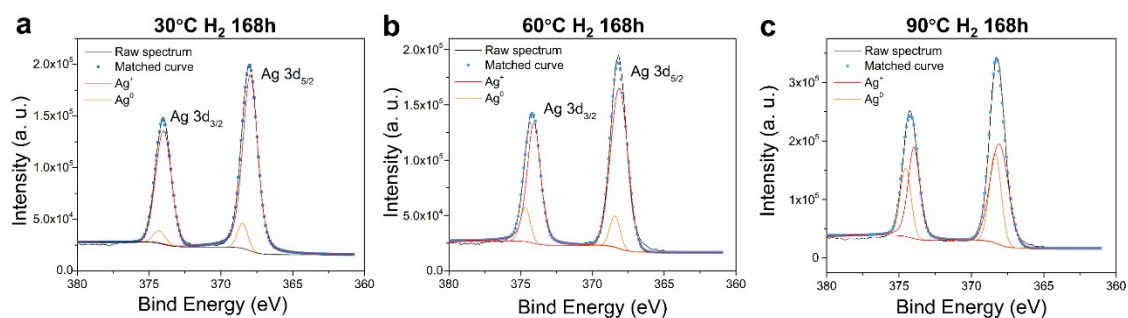


**Figure S30.** X-ray photoelectron spectroscopy (XPS) spectra of Ag in the Ag-60%IL@TpPa-SO<sub>3</sub>H membrane under hydrogen atmosphere for 168 h at 30, 60, and 90 °C, respectively. Charged compensation has been conducted for XPS data.

**Table S3.** Separation performance of the reported Supported Liquid Membranes for ethylene/ethane separation.

Membrane name	Measurement condition <sup>a</sup>	Selectivity	Permeance (GPU) <sup>b</sup>	Reference
Ag-DES	2 bar, mixed gas	27.33	5.92	1
GQD/RIL AMMM	1 bar, 25 °C, mixed gas	99.5	11.97 <sup>c</sup>	2
EIMN-GO	1 bar, 25 °C, mixed gas	215	72.5	3
EIMN-BN	1 bar, 25 °C, mixed gas	128	138	4
Ag/[Emim][Me <sub>2</sub> PO <sub>4</sub> ]	1.1 bar, 25 °C, mixed	35.8	0.979	5
Ag/[Emim][Et <sub>2</sub> PO <sub>4</sub> ]	gas	39.6	0.782	
[DMA·NO <sub>3</sub> ]-G and [TEA·NO <sub>3</sub> ]-G based FTMs	1.1 bar, 25 °C, mixed gas	70	1.9	6
		42	7.9	
		24	3.2	
		98	3.1	
		55	6.4	
		22	1	
		40.7	2.43	
		98.5	3.06	
		125.6	3.09	
		PIL-FTMs	1.1 bar, 25 °C, mixed gas	
25	0.55			
42	0.1			
15	0.55			
45	0.8			
PyAN	1.1 bar, 25 °C, mixed gas	57	2.44	8
		EIMN	51	
Trifluoromethanesulfonate and acetamide	1.1 bar, 25 °C, mixed gas	38	27.5	9
		45	17.5	
		62	7.68	

		48	4.12	
		12.5	0.123	
EG -DES	1.1 bar, 25 °C, mixed gas	6	0.28	10
		7	0.17	
		10	1.75	
CuCl/DESs-SLMs (ChCl:G)	1.1 bar, 25 °C, mixed gas	20	0.135	11
		10	0.085	
		11.5	0.09	
0.5[BMIM]Cl-CuCl-1/ 15ZnCl <sub>2</sub>	1.1 bar, 25 °C, mixed gas	17.8	0.286	12
		7	0.57	
		11	0.4	
CuCl and 1-butyl-3-methylimidazolium chloride	1.1 bar, 25 °C, pure gas	11.2	0.286	8
		9.8	0.326	
		5	0.837	
Ag-poly([pyrr11][NTf <sub>2</sub> ] and Ag-[pyr14][NTf <sub>2</sub> ])	1bar, 20°C, pure gas	3.21	0.184	13
		3.6	0.165	
		7.24	0.131	
		1.82	0.816	

- The measurement condition includes pressure, temperature, humidity (If the gas is humidified), and the pure or mixed gas. All pressures have been converted to absolute pressure in the unit of bar. And the unit of temperature has been converted into degree centigrade. For pure gas, the selectivity is ideal selectivity.
- The permeance refers to permeance of ethylene. All permeances have been converted into the unit of GPU. If the original unit is Barrer, the value will be divided by the membrane thickness ( $\mu\text{m}$ ).
- The thickness was not mentioned in the article and was at least 31  $\mu\text{m}$  estimated by SEM images.

**Table S4.** Separation performance of the reported Mixed Matrix Membranes for ethylene/ethane separation.

Membrane name	Measurement condition	Selectivity	Permeance (GPU)	Reference
HKUST-1@ODPA-TMPDA	35°C, mixed gas	3.4	0.19 <sup>a</sup>	14
HKUST-1@6FDA-TMPDA		2.4	2.18 <sup>b</sup>	
MOF801@Ni74(26)durene	1 bar, 35°C, pure gas	5.91	0.98 <sup>c</sup>	15
PFSA-PP_7/115_Ag	30°C, 50% humidity; mixed gas	12.11	39	16
20% Ni-gallate(F)/6FDA-DAM MMM	mixed gas	2.6	1.4	17
ZIF-8@DBzPBI-Bul	2.76 bar, 35 °C, pure gas	4.4	2.6	18
M <sub>2</sub> (dobdc)@6FDA-DAM	2 bar, 35 °C, pure gas	5	5.14	19
		4.7	9.42	
		2.7	29.14	
		2.3	12.85	
		4	4	
		3.8	3.8	
Cu3BTC2@P84	5 bar, mixed gas	7.1	1.00E-03	20, 21
Acetate-Silica@Cellulose	2 bar, 35 °C, pure gas	4.01	0.003	22
ZIF-8@poly(1,4-phenylene ether-ether-sulfone)	1bar, 25°C, pure gas	2	0.021	23
polyethylene-graftsulfonated polystyrene membranes	0.02 bar, 30% humidity, mixed gas	49	49	16
[C=O]:[Ag] as 1:1 and varying amounts of HBF <sub>4</sub>	42.76 bar, 25 °C, mixed gas	100	2.5	24
AgBF <sub>4</sub> @PA 12-PTMO	4.45 bar, 22 °C, mixed gas	26	20	25
Cu(1,3-butadiene)Otf@CA	1.38 bar, mixed gas	11	3.9	26

a, b. The thickness was not mentioned in the article and was about 84 μm estimated by SEM images.

c. The thickness was not mentioned in the article and was about 26.5 μm estimated by SEM images.

**Table S5.** Separation performance of the reported Polymeric and Carbon Molecular Sieve Membranes for ethylene/ethane separation.

Membrane name	Text condition	Selectivity	Permeance (GPU)	Reference
6FDA-polyimide	pure gas	2.5	1.2	17
6FDA-DAM:DABA(3:2)		4	0.14	
6FpDA:DABA CMS 576°C	4bar, 35°C, pure gas	4.8	4.08	27
6FpDA:DABA CMS 800°C		24.1	0.17	
6FDA-NDA	2 bar, 35°C, pure gas	6.84	0.023	28
6FDA-NDA/Durene (75:25)		5.62	0.089	
6FDA-NDA/Durene (50:50)		4.27	0.184	
6FDA-NDA/Durene (25:75)		3.6	0.734	
6FDA-Durene		2.89	1.534	
6FDA-mPD	3.8 bar, 35°C, pure gas	3.3	0.06	29
6FDA-IPDA		3.8	0.238	
		4.4	0.424	
PPO	1.77bar, 30°C, mixed gas (85% CH <sub>4</sub> , 5% C <sub>2</sub> H <sub>4</sub> , and 10% C <sub>2</sub> H <sub>6</sub> )	4.4	2	30
		5.3	2.3	
PPO Copolymer 1		2.9	1.1	
PPO Copolymer 2		4.8	0.41	
		4.5	0.83	
Polyethylene terephthalate		1.8	0.012	
PTFE		1.6	0.28	
MA4.8%-Air-150-550 (45 μm) (CMS)	20°C, pure gas	6.2	2.8	31
Matrimid-550 (59 μm) (CMS)		3.89	1.4	
FDA-DAM:DABA (3:2) polyimide (CMS)	35°C, mixed gas	11	0.125	32
spirobisindane-based polyimide (CMS)	2bar, 35°C, mixed gas	25	0.03	33
PIM-1 (CMS)	5bar, 35°C, mixed gas	9.7	0.274	34
PIM-1 (CMS)	2bar, 35°C, mixed gas	13	0.013	35
PIM-6FDA-OH (CMS)	50 psi (3.45 bar), 35°C, pure gas	14	0.12	36
PIM-6FDA-OH (CMS)	50 psi (3.45 bar), 35°C, mixed gas	7	0.74	
Matrimid® (CMS)	100 psig (7.9 bar), 35°C, pure gas	12	0.2	37
Matrimid® (CMS)	50 psi (3.45 bar), 35°C, pure gas	14	0.1	38
		10	0.25	
		4	1.8	
phenolic resin (CMS)	20 °C, pure gas	5.3	15	39
		3.2	5.5	

		1.5	4.5	
co-polyimide (BTDATDI/MDI) P84 (CMS)	2.1 bar, 25 °C, pure gas	9.1	110	40
		4	12	
		5.4	7	
		4.5	425	
phenolic resin (CMS)	1bar, 20 °C, pure gas	5.3	55	41
3,3,4,4'- biphenyltetracarboxylic dianhydride and aromatic diamines (CMS)	1bar, 100 °C, mixed gas	3.1	110	42
BPDA-pp'ODA polyimide (CMS)	1bar, 100 °C, pure gas	4.8	29.8	43

## Source Data

**Source Data 1.** Ethylene/ethane mixed gas separation performance of IL@TpPa-SO<sub>3</sub>H membranes (Figure 5a), including separation performance of each membrane, their average values and standard deviations.

Membrane Name	20%IL@TpPa-SO <sub>3</sub> H #1	20%IL@TpPa-SO <sub>3</sub> H #2	20%IL@TpPa-SO <sub>3</sub> H #3	Average Value	Standard Deviation
Ethylene Permeance (GPU)	342.52	344.94	330.30	342.52	9.14
Selectivity	1.43	1.38	1.41	1.41	0.02
Membrane Name	40%IL@TpPa-SO <sub>3</sub> H #1	40%IL@TpPa-SO <sub>3</sub> H #2	40%IL@TpPa-SO <sub>3</sub> H #3	Average Value	Standard Deviation
Ethylene Permeance (GPU)	167.79	176.05	153.19	165.68	9.45
Selectivity	1.45	1.66	1.85	1.66	0.16
Membrane Name	60%IL@TpPa-SO <sub>3</sub> H #1	60%IL@TpPa-SO <sub>3</sub> H #2	60%IL@TpPa-SO <sub>3</sub> H #3	Average Value	Standard Deviation
Ethylene Permeance (GPU)	73.80	74.69	75.20	74.56	0.58
Selectivity	1.96	1.95	1.97	1.96	0.01
Membrane Name	80%IL@TpPa-SO <sub>3</sub> H #1	80%IL@TpPa-SO <sub>3</sub> H #2		Average Value	Standard Deviation
Ethylene Permeance (GPU)	10.40	10.60		10.50	0.10
Selectivity	1.26	1.35		1.31	0.05
Membrane Name	100%IL@TpPa-SO <sub>3</sub> H #1	100%IL@TpPa-SO <sub>3</sub> H #2	100%IL@TpPa-SO <sub>3</sub> H #3	Average Value	Standard Deviation
Ethylene Permeance (GPU)	2.65	2.66	2.72	2.67	0.03
Selectivity	1.19	1.19	1.18	1.19	0.005

**Source Data 2.** Ethylene/ethane mixed gas separation performance of Ag-IL@TpPa-SO<sub>3</sub>H membranes (Figure 5b), including separation performance of each membrane, their average values and standard deviations.

Membrane Name	Ag-20%IL@TpPa-SO <sub>3</sub> H #1	Ag-20%IL@TpPa-SO <sub>3</sub> H #2	Ag-20%IL@TpPa-SO <sub>3</sub> H #3	Average Value	Standard Deviation
Ethylene Permeance (GPU)	273.13	215.57	233.36	240.69	29.47
Selectivity	5.05	5.07	7.21	5.78	1.24
Membrane Name	Ag-40%IL@TpPa-SO <sub>3</sub> H #1	Ag-40%IL@TpPa-SO <sub>3</sub> H #2	Ag-40%IL@TpPa-SO <sub>3</sub> H #3	Average Value	Standard Deviation
Ethylene Permeance (GPU)	172.06	158.82	140.14	157.01	16.04
Selectivity	27.49	29.62	27.29	28.11	1.29
Membrane Name	Ag-60%IL@TpPa-SO <sub>3</sub> H #1	Ag-60%IL@TpPa-SO <sub>3</sub> H #2	Ag-60%IL@TpPa-SO <sub>3</sub> H #3	Average Value	Standard Deviation
Ethylene Permeance (GPU)	105.53	114.02	105.99	108.51	4.78
Selectivity	121.77	110.28	106.43	112.83	7.98
Membrane Name	Ag-80%IL@TpPa-SO <sub>3</sub> H #1	Ag-80%IL@TpPa-SO <sub>3</sub> H #2	Ag-80%IL@TpPa-SO <sub>3</sub> H #3	Average Value	Standard Deviation
Ethylene Permeance (GPU)	37.36	36.82	38.99	37.72	1.13
Selectivity	21.79	17.89	20.00	19.78	1.95
Membrane Name	Ag-100%IL@TpPa-SO <sub>3</sub> H #1	Ag-100%IL@TpPa-SO <sub>3</sub> H #2	Ag-100%IL@TpPa-SO <sub>3</sub> H #3	Average Value	Standard Deviation
Ethylene Permeance (GPU)	8.47	8.39	8.51	8.46	0.07
Selectivity	17.27	18.34	20.88	18.72	1.85

**Source Data 3.** Ethylene/ethane pure gas separation performance of Ag-IL@TpPa-SO<sub>3</sub>H membranes (Figure S23), including separation performance of each membrane, their average values and standard deviations.

Membrane Name	Ag-20%IL@TpPa-SO <sub>3</sub> H #1	Ag-20%IL@TpPa-SO <sub>3</sub> H #2	Ag-20%IL@TpPa-SO <sub>3</sub> H #3	Average Value	Standard Deviation
Ethylene Permeance (GPU)	345.02	351.08	365.59	353.90	8.63
Selectivity	1.41	1.32	1.45	1.39	0.05
Membrane Name	Ag-40%IL@TpPa-SO <sub>3</sub> H #1	Ag-40%IL@TpPa-SO <sub>3</sub> H #2	Ag-40%IL@TpPa-SO <sub>3</sub> H #3	Average Value	Standard Deviation
Ethylene Permeance (GPU)	166.62	176.02	170.05	170.90	3.88
Selectivity	26.35	21.80	23.67	23.94	1.87
Membrane Name	Ag-60%IL@TpPa-SO <sub>3</sub> H #1	Ag-60%IL@TpPa-SO <sub>3</sub> H #2	Ag-60%IL@TpPa-SO <sub>3</sub> H #3	Average Value	Standard Deviation
Ethylene Permeance (GPU)	148.18	138.02	142.71	142.97	4.15
Selectivity	68.93	66.07	75.04	70.01	3.74
Membrane Name	Ag-80%IL@TpPa-SO <sub>3</sub> H #1	Ag-80%IL@TpPa-SO <sub>3</sub> H #2	Ag-80%IL@TpPa-SO <sub>3</sub> H #3	Average Value	Standard Deviation
Ethylene Permeance (GPU)	22.77	22.04	19.98	21.60	1.18
Selectivity	21.51	27.82	27.32	25.55	3.16
Membrane Name	Ag-100%IL@TpPa-SO <sub>3</sub> H #1	Ag-100%IL@TpPa-SO <sub>3</sub> H #2	Ag-100%IL@TpPa-SO <sub>3</sub> H #3	Average Value	Standard Deviation
Ethylene Permeance (GPU)	13.81	12.39	11.25	12.48	1.05
Selectivity	24.71	26.11	25.58	25.47	0.58

**Source Data 4.** Separation performance changes from test to stability of the Ag-60%IL@TpPa-SO<sub>3</sub>H membranes at initial stage of test (Figure S24), including the ethane permeance and selectivity of two test processes.

Time (min)	Text 1		Text 2	
	Ethane Permeance (GPU)	Selectivity	Ethane Permeance (GPU)	Selectivity
0	1.26	86.14	1.33	80.63
7	1.07	100.72	1.44	73.18
14	0.98	108.26	1.17	91.71
21	0.98	109.53	1.22	87.34
28	0.89	119.91	1.07	103.91
35	0.98	117.30	1.00	106.46
49	0.87	121.77	1.07	104.67

**Source Data 5.** The separation performance changes by temperature of the Ag-60%IL@TpPa-SO<sub>3</sub>H membranes (Figure S25), including separation performance of each membrane, their average values and standard deviations.

Temperature (°C)	20 #1	20 #2	20 #3	Average Value	Standard Deviation
Ethylene Permeance (GPU)	105.53	114.02	105.99	108.51	4.78
Selectivity	121.77	110.28	106.43	112.83	7.98
Temperature (°C)	25 #1	25 #2	25 #3	Average Value	Standard Deviation
Ethylene Permeance (GPU)	121.65	115.54	125.10	120.76	3.95
Selectivity	117.66	115.06	114.80	115.84	1.29
Temperature (°C)	30 #1	30 #2	30 #3	Average Value	Standard Deviation
Ethylene Permeance (GPU)	145.11	140.89	119.28	135.09	13.86
Selectivity	133.88	105.98	122.11	120.66	14.01
Temperature (°C)	35 #1	35 #2	35 #3	Average Value	Standard Deviation
Ethylene Permeance (GPU)	125.89	126.94	128.64	127.16	1.13
Selectivity	108.10	102.31	102.29	104.23	2.73
Temperature (°C)	40 #1	40 #2	40 #3	Average Value	Standard Deviation
Ethylene Permeance (GPU)	122.96	120.99	121.17	121.71	1.09
Selectivity	94.75	103.45	111.05	99.10	8.15
Temperature (°C)	50 #1	50 #2	50 #3	Average Value	Standard Deviation
Ethylene Permeance (GPU)	90.98	88.63	87.54	89.05	1.76
Selectivity	83.62	114.15	93.58	97.12	15.57
Temperature (°C)	60 #1	60 #2	60 #3	Average Value	Standard Deviation
Ethylene Permeance (GPU)	100.37	96.06	98.07	98.17	2.16
Selectivity	74.39	80.69	105.86	86.98	16.65
Temperature (°C)	70 #1	70 #2	70 #3	Average Value	Standard Deviation
Ethylene Permeance (GPU)	83.35	80.93	85.52	83.27	1.87
Selectivity	79.17	78.02	77.65	78.28	0.65

**Source Data 6.** Propylene/propane mixed gas separation performance of Ag-IL@TpPa-SO<sub>3</sub>H membranes (Figure S27), including separation performance of each membrane, their average values and standard deviations.

Membrane Name	Ag-20%IL@TpPa-SO <sub>3</sub> H #1	Ag-20%IL@TpPa-SO <sub>3</sub> H #2	Ag-20%IL@TpPa-SO <sub>3</sub> H #3	Average Value	Standard Deviation
Propylene Permeance (GPU)	166.96	184.92	188.12	180.00	11.41
Selectivity	7.17	7.40	7.27	7.28	0.12
Membrane Name	Ag-40%IL@TpPa-SO <sub>3</sub> H #1	Ag-40%IL@TpPa-SO <sub>3</sub> H #2	Ag-40%IL@TpPa-SO <sub>3</sub> H #3	Average Value	Standard Deviation
Propylene Permeance (GPU)	87.48	78.21	82.42	82.70	4.64
Selectivity	89.58	94.08	98.58	90.74	4.50
Membrane Name	Ag-60%IL@TpPa-SO <sub>3</sub> H #1	Ag-60%IL@TpPa-SO <sub>3</sub> H #2	Ag-60%IL@TpPa-SO <sub>3</sub> H #3	Average Value	Standard Deviation
Propylene Permeance (GPU)	17.99	17.35	17.20	17.51	0.42
Selectivity	37.89	41.53	40.54	39.99	1.88
Membrane Name	Ag-80%IL@TpPa-SO <sub>3</sub> H #1	Ag-80%IL@TpPa-SO <sub>3</sub> H #2	Ag-80%IL@TpPa-SO <sub>3</sub> H #3	Average Value	Standard Deviation
Propylene Permeance (GPU)	11.85	11.54	12.02	11.80	0.24
Selectivity	24.68	23.18	24.32	24.05	0.78
Membrane Name	Ag-100%IL@TpPa-SO <sub>3</sub> H #1	Ag-100%IL@TpPa-SO <sub>3</sub> H #2	Ag-100%IL@TpPa-SO <sub>3</sub> H #3	Average Value	Standard Deviation
Propylene Permeance (GPU)	5.43	5.71	5.54	5.56	0.14
Selectivity	26.03	34.62	35.26	31.97	5.16

**Source Data 7.** Separation performance of long-term stability of Ag-60%IL@TpPa-SO<sub>3</sub>H membrane (Figure 6a).

Time (h)	C <sub>2</sub> H <sub>4</sub> permeance (GPU)	C <sub>2</sub> H <sub>6</sub> permeance (GPU)	Selectivity
0.00	129.21	0.92	141.11
12.00	123.76	1.09	114.02
24.00	128.64	1.14	112.38
36.00	137.88	1.17	118.14
48.00	138.98	1.14	122.27
60.00	147.79	1.17	126.37
72.00	135.78	1.14	119.36
84.00	134.01	1.07	124.68
96.00	136.01	0.91	149.25
108.00	141.79	1.06	133.18
120.00	140.79	1.23	114.66
132.00	131.24	1.07	122.27
144.00	133.08	0.90	147.08
156.00	118.49	0.82	144.27
168.00	124.88	0.95	132.11

**Source Data 8.** Separation performance of Ag-60%IL@TpPa-SO<sub>3</sub>H membranes exposed to hydrogen (Figure 6b).

Time (h)	C <sub>2</sub> H <sub>4</sub> permeance (GPU)	C <sub>2</sub> H <sub>6</sub> permeance (GPU)	Selectivity
0.00	124.21	0.88	141.93
24.00	132.41	1.00	131.96
48.00	145.65	1.55	94.24
72.00	141.49	1.11	127.78
96.00	138.51	1.17	118.53
120.00	143.85	1.04	138.29
144.00	132.32	1.09	121.28
168.00	129.09	1.03	125.57

**Source Data 9.** Separation performance of Ag-60%IL@TpPa-SO<sub>3</sub>H membranes exposed to hydrogen at 60 and 90 °C (Figure S29).

Time (h)	60 °C		90 °C	
	C <sub>2</sub> H <sub>4</sub> Permeance (GPU)	C <sub>2</sub> H <sub>4</sub> / C <sub>2</sub> H <sub>6</sub> Selectivity	C <sub>2</sub> H <sub>4</sub> Permeance (GPU)	C <sub>2</sub> H <sub>4</sub> / C <sub>2</sub> H <sub>6</sub> Selectivity
0	129.45	135.83	135.93	132.97
24	126.65	118.16	113.89	104.71
72	118.73	100.8	105.76	78.66
120	118.62	92.52	82.34	63.01
168	98.99	87.45	57.55	23.58

**Source Data 10.** The separation performance of the Ag-60%IL@TpPa-SO<sub>3</sub>H membranes under variable pressure from 1 to 7 bar (Figure 6c).

Pressure (bar)	Ethylene permeance (GPU)	Selectivity
1.0	130.13	124.6
1.5	131.65	115.3
2.0	112.13	111.4
2.5	106.2	113.1
3.0	107.47	110.21
3.5	103.65	104.15
4.0	98.23	96.39
4.5	100.21	89.46
5.0	94.18	78.77
5.5	88.22	73.4
6.0	87.62	68.13
6.5	81.89	30.77
7.0	108.15	6.89

## References

1. B. Jiang, J. Zhou, M. Xu, H. Dou, H. Zhang, N. Yang and L. Zhang, *J. Membr. Sci.*, 2020, **610**, 118243.
2. H. Dou, M. Xu, B. Wang, Z. Zhang, D. Luo, B. Shi, G. Wen, M. Mousavi, A. Yu, Z. Bai, Z. Jiang and Z. Chen, *Angew. Chem. Int. Ed.*, 2021, **60**, 5864-5870.
3. H. Dou, M. Xu, B. Jiang, G. Wen, L. Zhao, B. Wang, A. Yu, Z. Bai, Y. Sun, L. Zhang, Z. Chen and Z. Jiang, *Adv. Funct. Mater.*, 2019, **29**, 1905229.
4. H. Dou, B. Jiang, M. Xu, Z. Zhang, G. Wen, F. Peng, A. Yu, Z. Bai, Y. Sun, L. Zhang, Z. Jiang and Z. Chen, *Angew. Chem. Int. Ed.*, 2019, **58**, 13969-13975.
5. H. Dou, B. Jiang, M. Xu, J. Zhou, Y. Sun and L. Zhang, *Chem. Eng. Sci.*, 2019, **193**, 27-37.
6. H. Dou, B. Jiang, L. Zhang, M. Xu and Y. Sun, *J. Membr. Sci.*, 2018, **567**, 39-48.
7. H. Dou, B. Jiang, X. Xiao, M. Xu, B. Wang, L. Hao, Y. Sun and L. Zhang, *J. Membr. Sci.*, 2018, **557**, 76-86.
8. H. Dou, B. Jiang, X. Xiao, M. Xu, X. Tantai, B. Wang, Y. Sun and L. Zhang, *ACS Appl. Mater. Interfaces*, 2018, **10**, 13963-13974.
9. B. Jiang, H. Dou, B. Wang, Y. Sun, Z. Huang, H. Bi, L. Zhang and H. Yang, *ACS sustainable chem. eng.*, 2017, **5**, 6873-6882.
10. R. Deng, Y. Sun, H. Bi, H. Dou, H. Yang, B. Wang, W. Tao and B. Jiang, *Energy Fuels*, 2017, **31**, 11146-11155.
11. B. Jiang, H. Dou, L. Zhang, B. Wang, Y. Sun, H. Yang, Z. Huang and H. Bi, *J. Membr. Sci.*, 2017, **536**, 123-132.
12. B. Jiang, W. Tao, H. Dou, Y. Sun, H. Xiao, L. Zhang and N. Yang, *Ind. Eng. Chem. Res.*, 2017, **56**, 15153-15162.
13. L. C. Tome, D. Mecerreyes, C. S. R. Freire, L. P. N. Rebelo and I. M. Marrucho, *J. Mater. Chem. A*, 2014, **2**, 5631-5639.
14. C. Y. Chuah, S. A. S. C. Samarasinghe, W. Li, K. Goh and T.-H. Bae, *Membranes*, 2020, **10**, 74.
15. C. Wu, K. Zhang, H. Wang, Y. Fan, S. Zhang, S. He, F. Wang, Y. Tao, X. Zhao, Y.-B. Zhang, Y. Ma, Y. Lee and T. Li, *J. Am. Chem. Soc.*, 2020, **142**, 18503-18512.
16. A. O. Volkov, D. V. Golubenko and A. B. Yaroslavtsev, *Sep. Purif. Technol.*, 2021, **254**, 117562.
17. G. Chen, X. Chen, Y. Pan, Y. Ji, G. Liu and W. Jin, *J. Membr. Sci.*, 2021, **620**, 118852.
18. S. H. Kunjattu, V. Ashok, A. Bhaskar, K. Pandare, R. Banerjee and U. K. Kharul, *J. Membr. Sci.*, 2018, **549**, 38-45.
19. J. E. Bachman, Z. P. Smith, T. Li, T. Xu and J. R. Long, *Nat. Mater.*, 2016, **15**, 845-849.
20. J. Ploegmakers, S. Japip and K. Nijmeijer, *J. Membr. Sci.*, 2013, **428**, 331-340.
21. J. Ploegmakers, S. Japip and K. Nijmeijer, *J. Membr. Sci.*, 2013, **428**, 445-453.
22. M. Naghsh, M. Sadeghi, A. Moheb, M. P. Chenar and M. Mohagheghian, *J. Membr. Sci.*, 2012, **423**, 97-106.
23. K. Diaz, M. Lopez-Gonzalez, L. F. del Castillo and E. Riande, *J. Membr. Sci.*, 2011, **383**, 206-213.
24. J. H. Kim, B. R. Min, H. S. Kim, J. Won and Y. S. Kang, *J. Membr. Sci.*, 2003, **212**, 283-288.
25. A. Morisato, Z. J. He, I. Pinnau and T. C. Merkel, *Desalination*, 2002, **145**, 347-351.

26. H. S. Kim, Y. J. Kim, J. J. Kim, S. D. Lee, Y. S. Kang and C. S. Chin, *Chem. Mater.*, 2001, **13**, 1720-1725.
27. Q. Wang, F. Huang, C. J. Cornelius and Y. Fan, *J. Membr. Sci.*, 2021, **621**, 118785.
28. S. S. Chan, T.-S. Chung, Y. Liu and R. Wang, *J. Membr. Sci.*, 2003, **218**, 235-245.
29. C. Staudt-Bickel and W. J. Koros, *J. Membr. Sci.*, 2000, **170**, 205-214.
30. O. M. Ilinitch, G. L. Semin, M. V. Chertova and K. I. Zamaraev, *J. Membr. Sci.*, 1992, **66**, 1-8.
31. J. Liu, J. Goss, T. Calverley, G. Meyers, M. A. Thorseth, C. S. Todd, J. Kang, A. Denise, H. Clements, J. Klann, K. Mabe, L. Xu, M. Brayden and M. Martinez, *J. Membr. Sci.*, 2020, **615**, 118554.
32. Y.-H. Chu, D. Yancey, L. Xu, M. Martinez, M. Brayden and W. Koros, *J. Membr. Sci.*, 2018, **548**, 609-620.
33. O. Salinas, X. Ma, Y. Wang, Y. Han and I. Pinnau, *RSC Adv.*, 2017, **7**, 3265-3272.
34. K.-S. Liao, S. Japip, J.-Y. Lai and T.-S. Chung, *J. Membr. Sci.*, 2017, **534**, 92-99.
35. O. Salinas, X. Ma, E. Litwiller and I. Pinnau, *J. Membr. Sci.*, 2016, **504**, 133-140.
36. O. Salinas, X. Ma, E. Litwiller and I. Pinnau, *J. Membr. Sci.*, 2016, **500**, 115-123.
37. M. Rungta, L. Xu and W. J. Koros, *Carbon*, 2012, **50**, 1488-1502.
38. L. Xu, M. Rungta and W. J. Koros, *J. Membr. Sci.*, 2011, **380**, 138-147.
39. T. A. Centeno, J. L. Vilas and A. B. Fuertes, *J. Membr. Sci.*, 2004, **228**, 45-54.
40. J. N. Barsema, N. F. A. van der Vegt, G. H. Koops and M. Wessling, *J. Membr. Sci.*, 2002, **205**, 239-246.
41. A. B. Fuertes and I. Menendez, *Sep. Purif. Technol.*, 2002, **28**, 29-41.
42. K. Okamoto, S. Kawamura, M. Yoshino, H. Kita, Y. Hirayama, N. Tanihara and Y. Kusuki, *Ind. Eng. Chem. Res.*, 1999, **38**, 4424-4432.
43. J.-i. Hayashi, H. Mizuta, M. Yamamoto, K. Kusakabe, S. Morooka and S.-H. Suh, *Ind. Eng. Chem. Res.*, 1996, **35**, 4176-4181.